Science Advances
AAAS

Supplementary Materials for

In vivo peptide-based delivery of a gene-modifying enzyme into cells of the central nervous system

Jason K. Allen *et al.*

Corresponding author: Jean-Philippe Pellois, pellois@tamu.edu; Cédric G. Geoffroy, geoffroy@tamu.edu

Sci. Adv. **8**, eabo2954 (2022)
DOI: 10.1126/sciadv.abo2954

This PDF file includes:

Figure S1

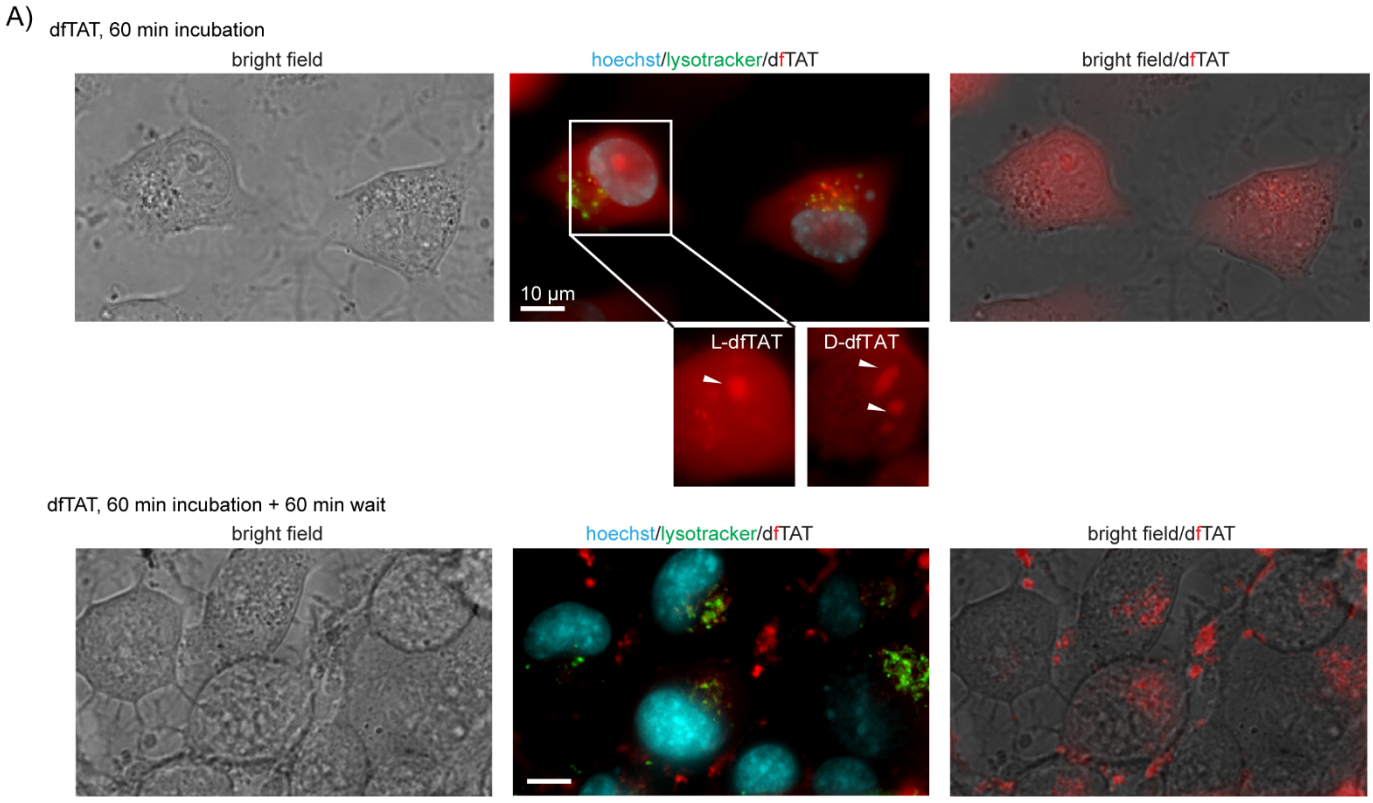
A)
dfTAT, 60 min incubation
bright field
hoechst/lysotracker/dfTAT
bright field/dfTAT
10 µm
L-dfTAT
D-dfTAT
dfTAT, 60 min incubation + 60 min wait
bright field
hoechst/lysotracker/dfTAT
bright field/dfTAT

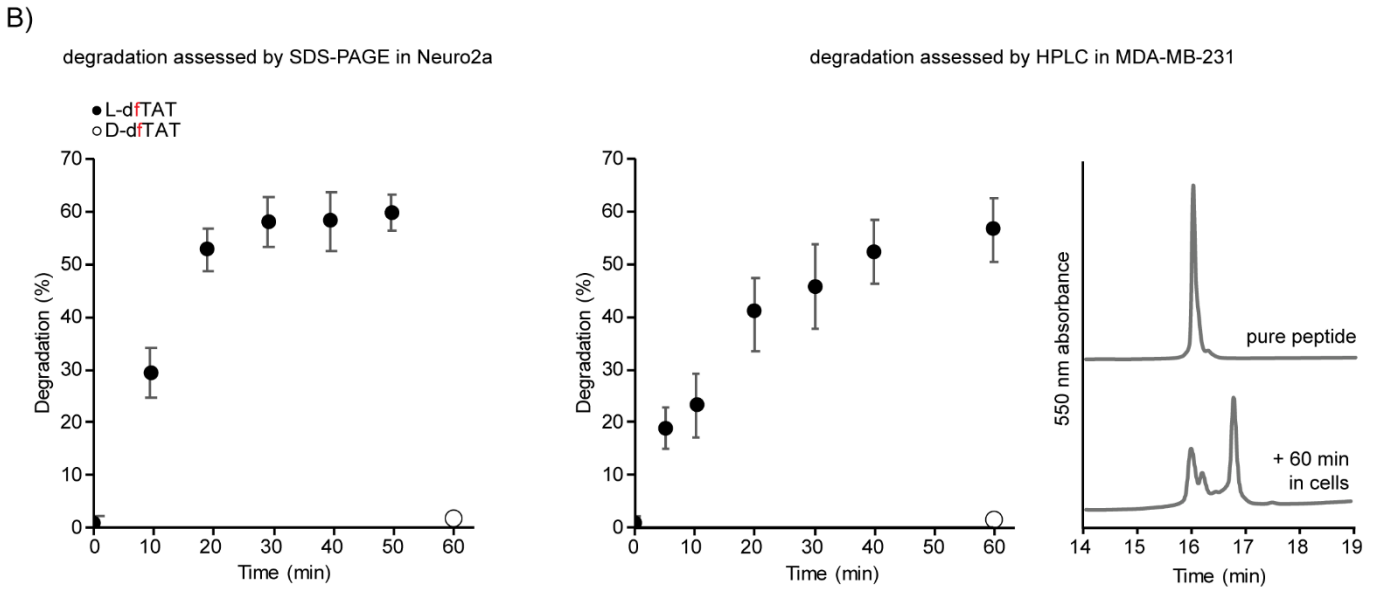
B)
degradation assessed by SDS-PAGE in Neuro2a
degradation assessed by HPLC in MDA-MB-231
L-dfTAT
D-dfTAT
Degradation (%)
Time (min)
550 nm absorbance
pure peptide
+ 60 min
in cells

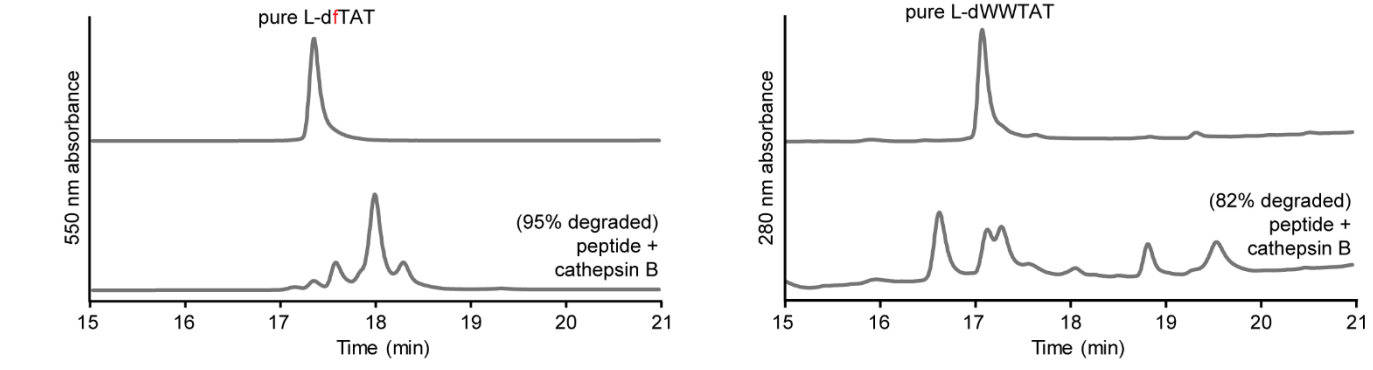
C)
pure L-dfTAT
550 nm absorbance
(95% degraded)
peptide +
cathepsin B
Time (min)
pure L-dWWTAT
280 nm absorbance
(82% degraded)
peptide +
cathepsin B
Time (min)

Figure S1. Peptide degradation. A) Fluorescence images of Neuro2a cells incubated with 5 μM dfTAT for 60 min and imaged after 5 or 60 min wait. Zoom-in images of L-dfTAT and D-dfTAT show distinct nucleolar staining. B) Cells were lysed from individual wells at the indicated time points for analysis of peptide degradation by either SDS-PAGE densitometry or by HPLC. Degradation was measured in biological duplicate on two different days. C) Degradation of dfTAT and d(WW)TAT *in vitro* by the prominent lysosomal protease cathepsin B as measured by HPLC.

Figure S2

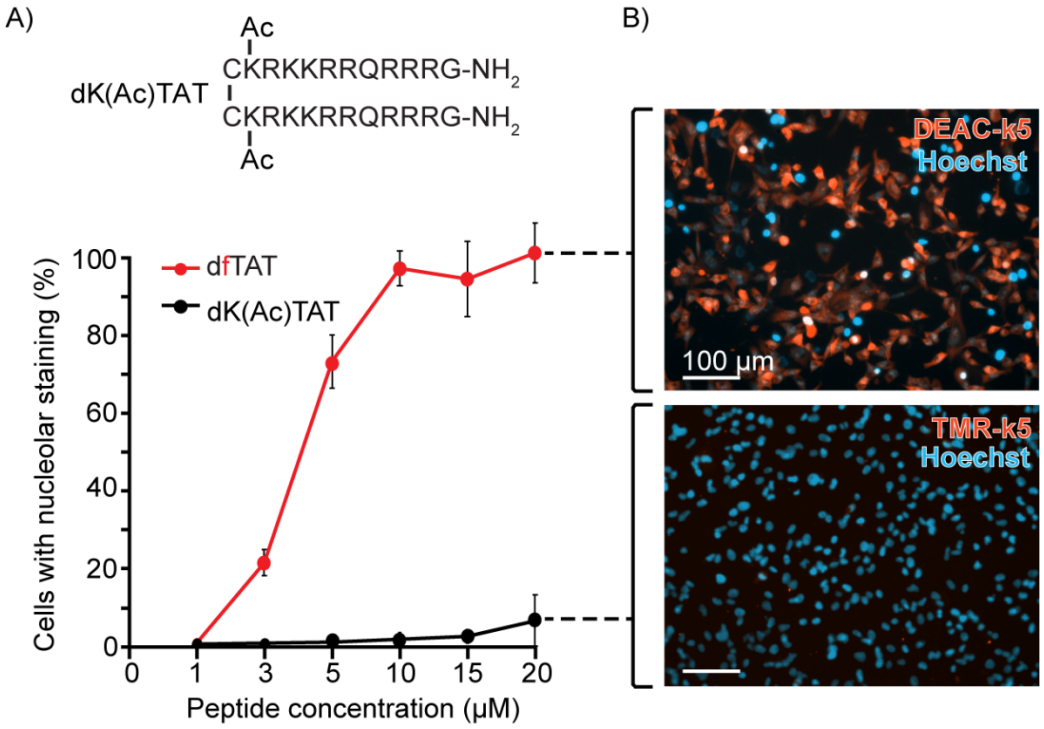

Figure S2. The "X" position is critical for activity. A) The sequence and structure of the dK(Ac)TAT peptide. Quantified delivery of pentalysine probes (DEAC-k5 or TMR-k5) by the fluorescent dfTAT peptide and the dK(Ac)TAT peptide. The DEAC-k5 peptide was used in place of TMR-k5 for the dfTAT condition due to dfTAT also being labeled with tetramethylrhodamine. Cells were quantified based on the distinct nucleolar staining of the pentalysine probes. B) Qualitative images of the pentalysine probe fluorescence in MDA-MB-231 cells as delivered by either dfTAT or dK(Ac)TAT. The DEAC-k5 is pseudocolored red to allow for the Hoechst channel to remain cyan in both images. These data were derived from biological triplicates conducted over three different days.

Figure S3

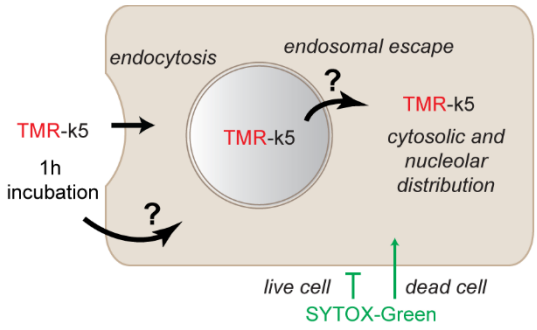

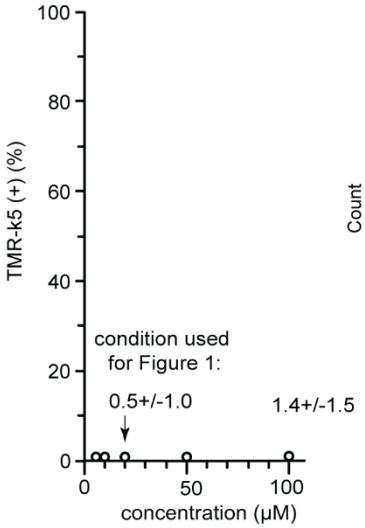

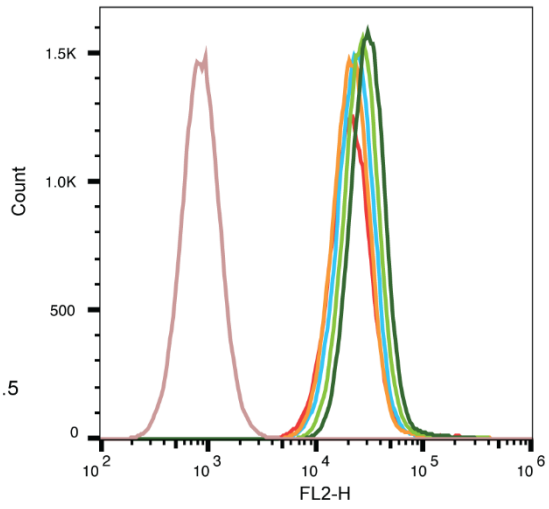

TMR-k5	Count	Median	SYTOX(+) (%)
0 μM	43k	872	1+/-0.5
5 μM	38k	21192	1+/-0.5
10 μM	42k	21577	1+/-0.5
20 μM	42k	23660	1+/-0.5
50 μM	42k	26715	1+/-0.5
100 μM	42k	30574	1+/-0.5

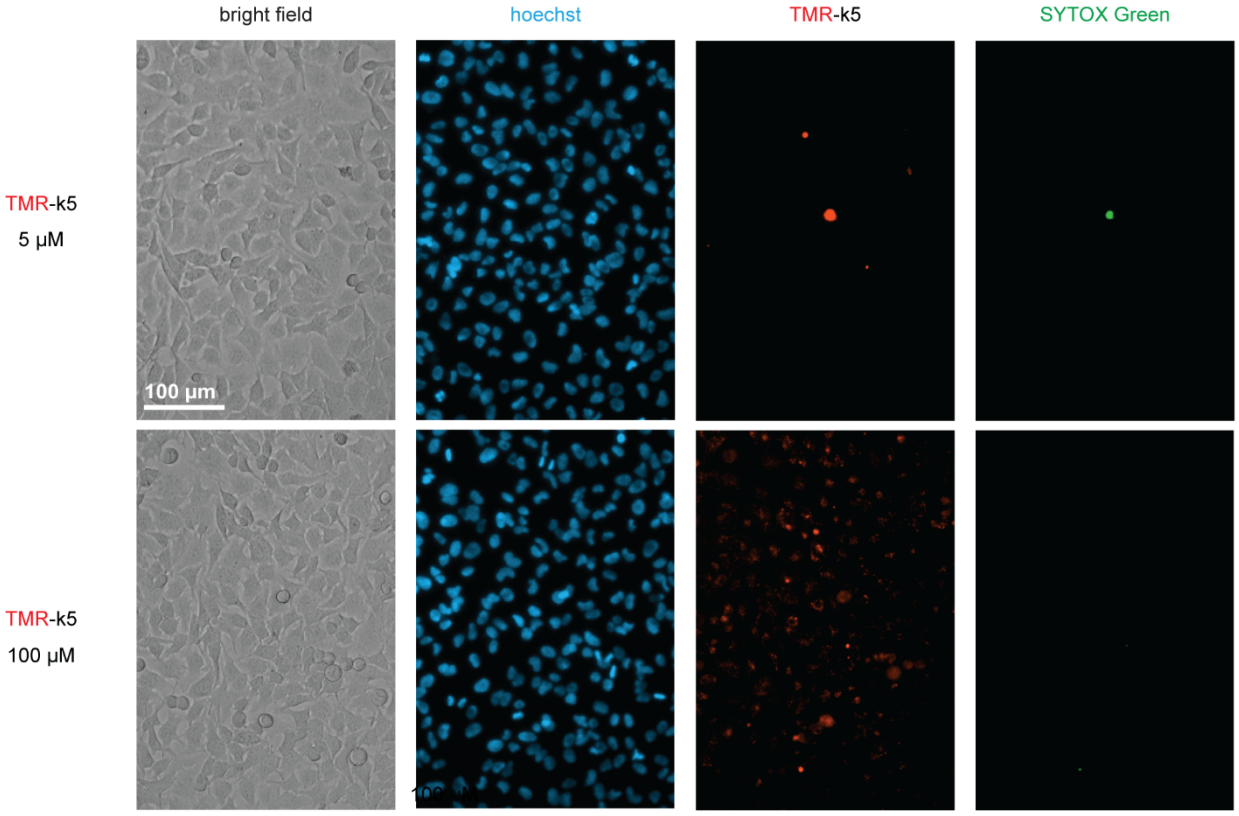

Figure S3. TMR-k5 uptake and penetration. HeLa cells were treated with increasing levels of TMR-k5 for 1 hour and uptake was measured by flow cytometry. A slight increase in total uptake of TMR-k5 was observed for increasing incubation concentrations. Fluorescence microscopy shows that TMR-k5 is not toxic at concentrations as high as 100 μM and is also unable to penetrate cells on its own as indicated by the absence of nucleolar staining.

Figure S4

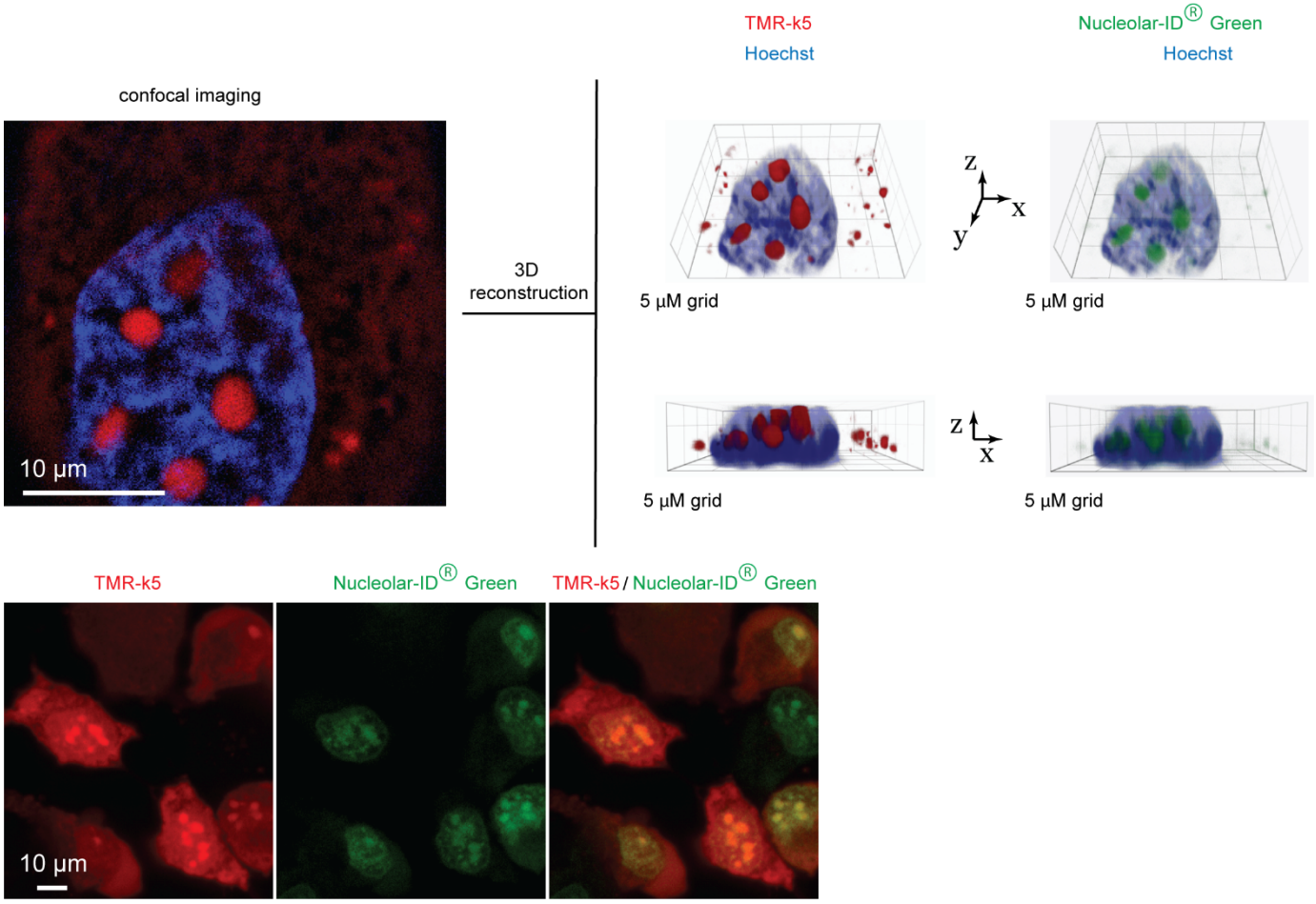

Figure S4. TMR-k5 stains nucleoli. Confocal imaging of cells stained by TMR-k5. Hela cells were treated with TMR-k5 (20 µM) and d(WW)TAT (2.5 µM) for 1h. Cells were washed and stained with Nucleolar-ID® Green (Enzo Life Sciences) and Hoechst. Images were acquired at 0.2 µm intervals on the z-axis using a disk-spinning unit (IX2-DSU) on a IX81 Olympus microscope. Z-stack images were reconstructed into a 3D view using Slidebook 6.0 3D view module. Images provided are 2D or 3D reconstructions with TMR-k5 pseudocolored red, Nucleolar-ID® Green pseudocolored green, and Hoechst pseudocolored blue. The contrast of TMR-k5 fluorescence in 3D reconstructions was adjusted to remove the contribution of cytoplasmic/nuclear diffused fluorescence which is lower than the signal in nucleoli, and in endosomes (as seen in puncta outside cells). The TMR-k5-stained intranuclear compartments are contained within Hoechst-stained volumes and co-localize with Nucleolar-ID® Green compartments both in 2D images (seen as yellow in red + green overlay) and 3D reconstructions. We conclude that these TMR-k5-stained intranuclear compartments are nucleoli.

Figure S5

initial experiment, microscope specific:

test d(X)TAT delivery at different TMR-k5 concentrations to get fluorescence signal that is detectable in >90% cells (chose 20 μM)

↓

determine exposure time and light intensity that yields highest intensity without pixel saturation (image whole dish)

↓

use 20 μM TMR-5 and same exposure time/light intensity/gain for all d(X)TAT delivery experiments (cells stained with Hoechst and SYTOX)

for each experiment (change [d(X)TAT] and test different peptides):

Image Hoechst, TMR-k5, SYTOX

↓

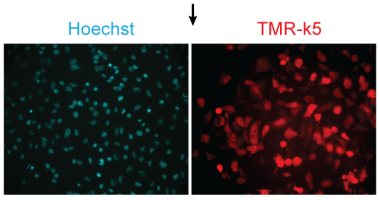

↓

identify nuclei from Hoechst image (parent image, Celleste software)

↓

exclude SYTOX positive cells

↓

identify nuclei in TMR-k5 image from Hoechst parent images, SYTOX (+) nuclei excluded

↓

measure fluorescence intensity of nuclei in TMR-k5 image

↓

process multiple images, ~3000-5000 cells per conditions

↓

count nuclei stained with TMR-k5

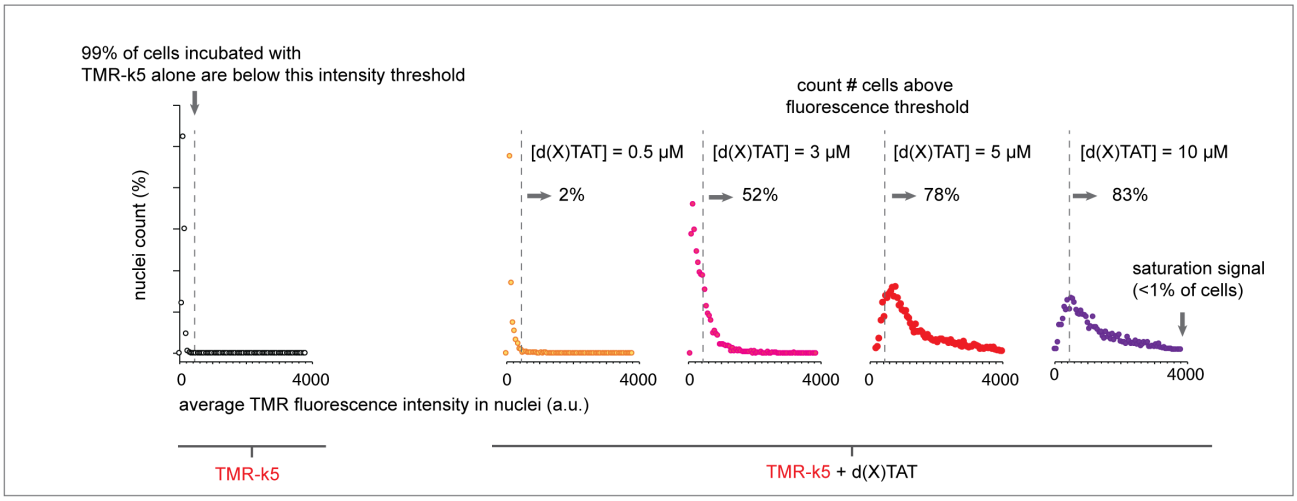

↓

visually examine cells to confirm presence of stained nucleoli (nucleoli negative cells are ruled out, <1% of total)

confirm nuclear localization with colocalization intersect with Hoechst (see AF488-H1 processing)

↓

TMR-k5 (+) (%) = cells with nuclei/nucleoli stained by TMR-k5 (% of total)

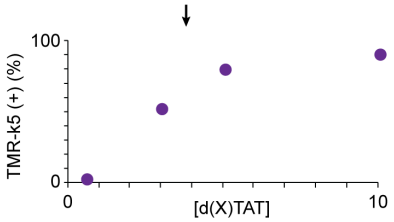

↓

triplicate, report average and standard deviation

Figure S5. Quantification protocol of TMR-k5 delivery. Scheme illustrating the general protocol used to quantify the number of cells displaying TMR-k5 nuclear/nucleolar staining after delivery with d(X)TAT reagents. The methods are described in Materials and Methods. Herein, we give examples of data obtained after incubation of Neuro2a with TMR-k5 (20 μM) and d(LL)TAT (0.5-10 μM). Hoechst staining is used to identify nuclei and the TMR-k5 fluorescence signal in nuclei is then quantified. Cells incubated with TMR-k5 alone are used to establish a nuclear fluorescence background threshold. The number of cells incubated with TMR-k5/d(LL)TAT containing nuclear red fluorescence above this determined threshold is counted. TMR-k5 nuclear staining is then confirmed by visually examining each cell for nucleolar staining (we have not yet found a reliable way to automate this step; the presence of bright intranuclear compartments approximately 2 μm in diameter is used as criteria for a positive signal (see Figure S4). Nucleolar staining is used to validate that the fluorescence signal is intranuclear and therefore intracellular (as opposed to diffuse and out-of-focus extracellular signal). The colocalization intersect of Hoechst and TMR-k5 (see description in Figure S10, same method used for Hoechst/AF488-H1colocalization intersect) is also used to confirm that the TMR-k5 nuclear signal does not originate from endosomal puncta overlapping with the Hoechst-defined region.

Figure S6

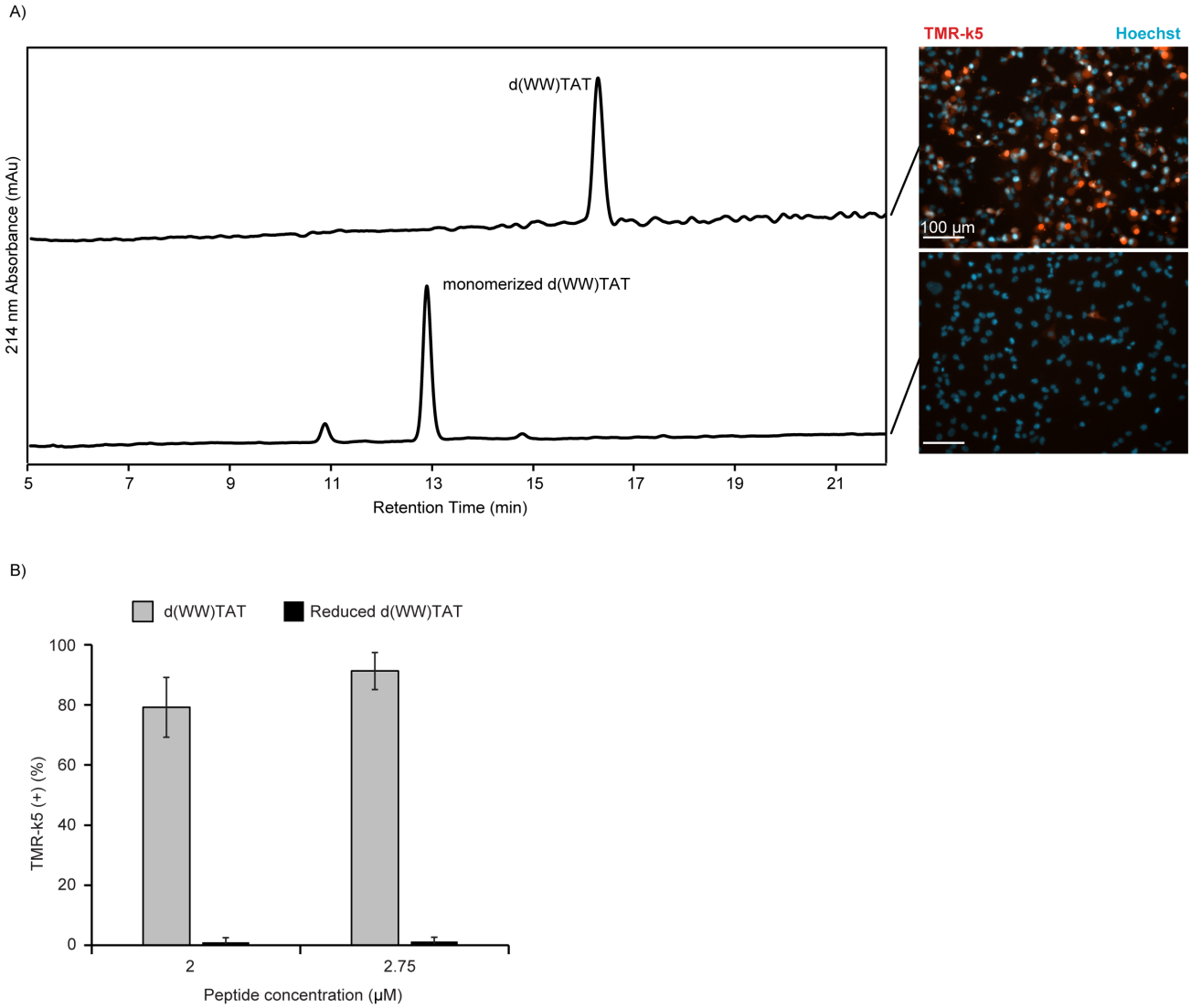

Figure S6. Peptide dimers of the d(X)TAT format show a near complete loss of activity when in their monomeric form. A) Analytical HPLC traces of the d(WW)TAT peptide before and after reduction of the dimer by incubation with L-cysteine for 30 min. The resulting peptide cocktails were incubated with MDA-MB-231 cells. Reducing the peptide results in almost complete abrogation of TMR-k5 delivery as shown qualitatively via fluorescence microscopy (right). B) Quantitation of fluorescence microscopy images. These data were derived from biological duplicates on two different days.

Figure S7

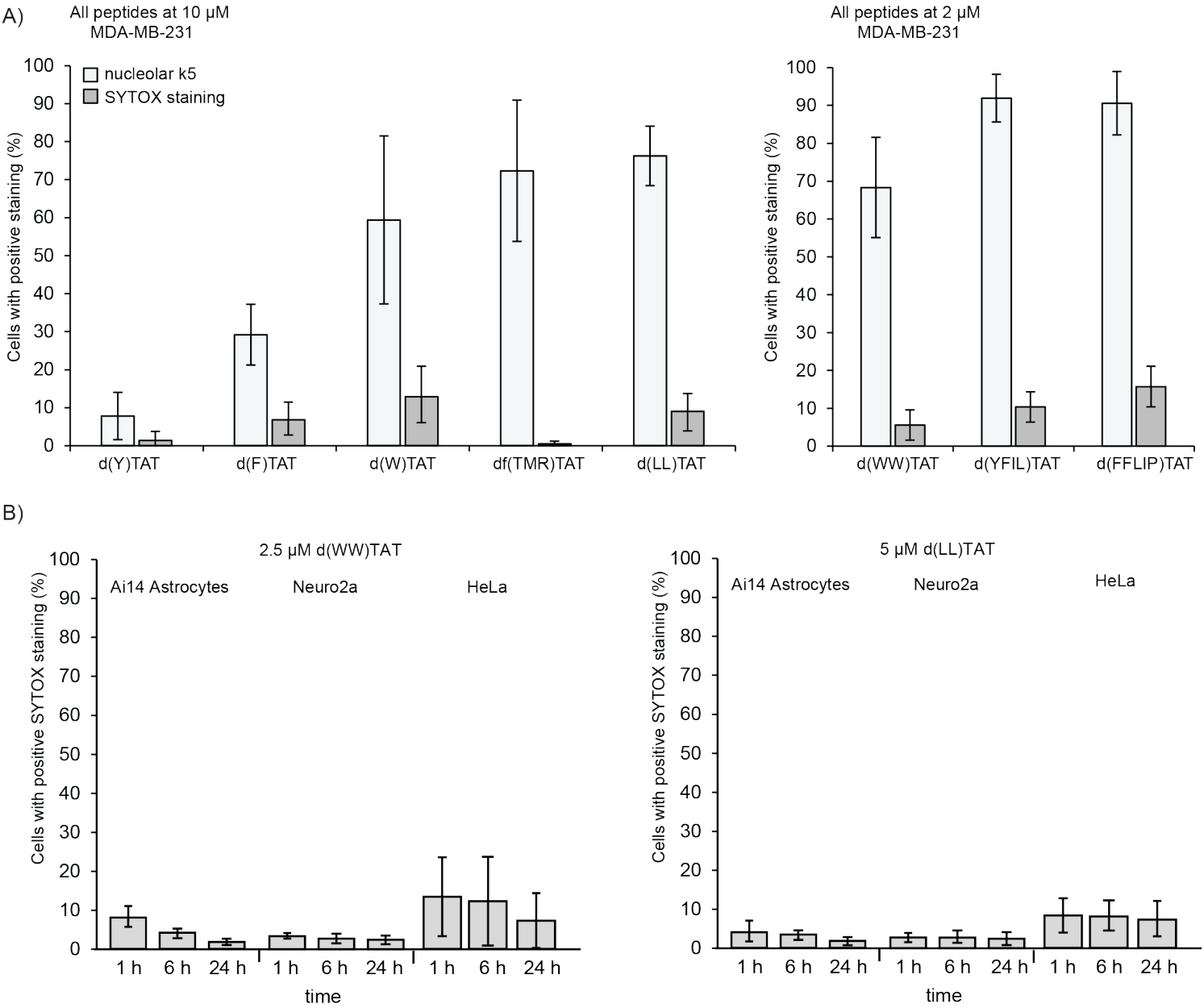

Figure S7. Relative toxicity of d(X)TAT towards several cell lines. A) Quantification of d(X)TAT delivery and toxicity in MDA-MB-231. MDA-MB-231 cells were exposed to d(X)TAT peptides at the concentrations indicated for 1 h. Delivery was assessed immediately after incubation as described in Figure 1. Toxicity was quantified by counting the number of cells stained with the live/dead cell reporter SYTOX Green by fluorescence microscopy. Cells positive for SYTOX staining are considered dead and not counted as positive for delivery of k5. Conversely, cells counted as positive for k5 delivery are not stained by SYTOX. B) Toxicity of d(WW)TAT or d(LL)TAT in primary Ai14 astrocytes, Neuro2a, and HeLa. Cells were incubated with the peptides for 1h, and toxicity was measured at the time indicated by detection of SYTOX green staining.

Figure S8

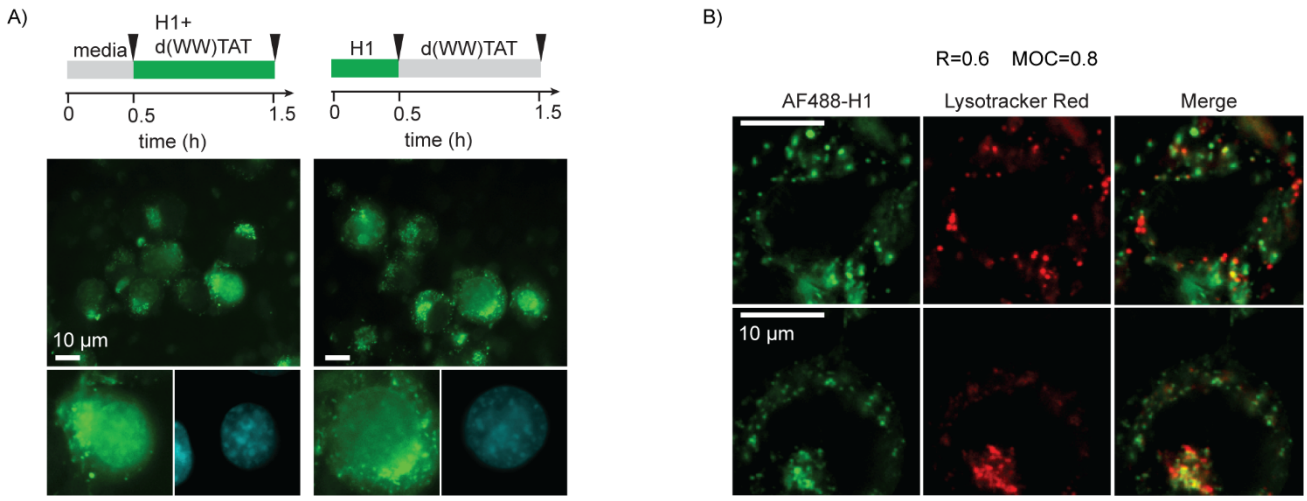

Figure S8. AF488-H1 delivery by d(WW)TAT. A) Delivery of AF488-H1 by d(WW)TAT in the co-incubation or preincubation formats indicated. Representative fluorescence images are provided, AF488-H1 being pseudocolored green and Hoechst cyan. B) Representative fluorescence images through which the Pearson's colocalization coefficient (R) and Mander's overlap coefficient (MOC) were calculated for AF488-H1 alone. Histone highly colocalizes with Lysotracker Red indicating endosomal entrapment.

Figure S9

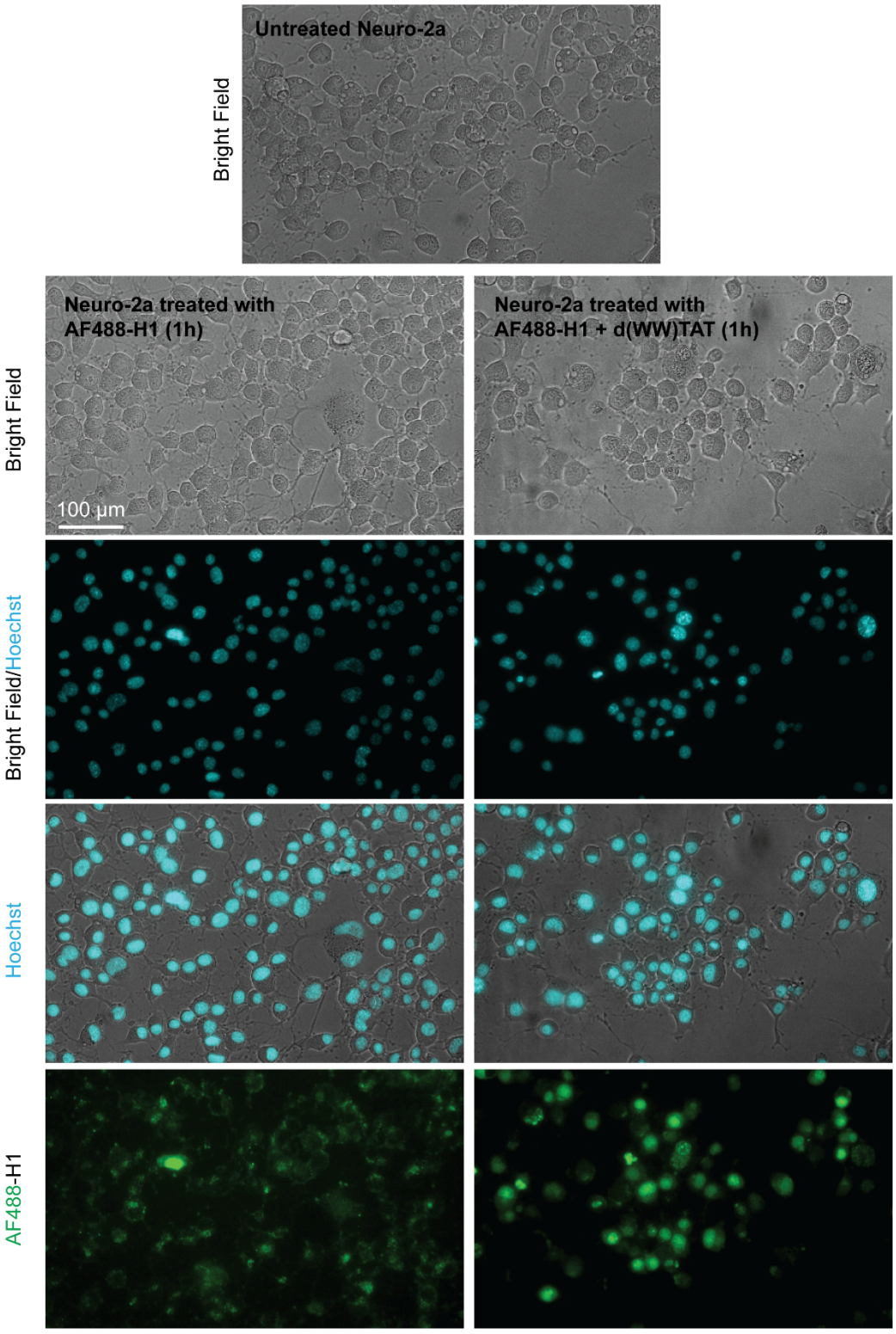

Figure S9. Qualitative images of AF488-H1 delivery. 20X images of Neuro2a cells, untreated, treated for 1 h with AF488-H1 (0.75 μM), and treated for 1 h with AF488-H1 (0.75 μM) and d(WW)TAT (2.5 μM). Cells were washed and stained with Hoechst. Cells were then imaged using 20X magnification in the bright field, CFP, and GFP channels. The fluorescence images are pseudo colored cyan for Hoechst and green for AF488-H1.

Figure S10

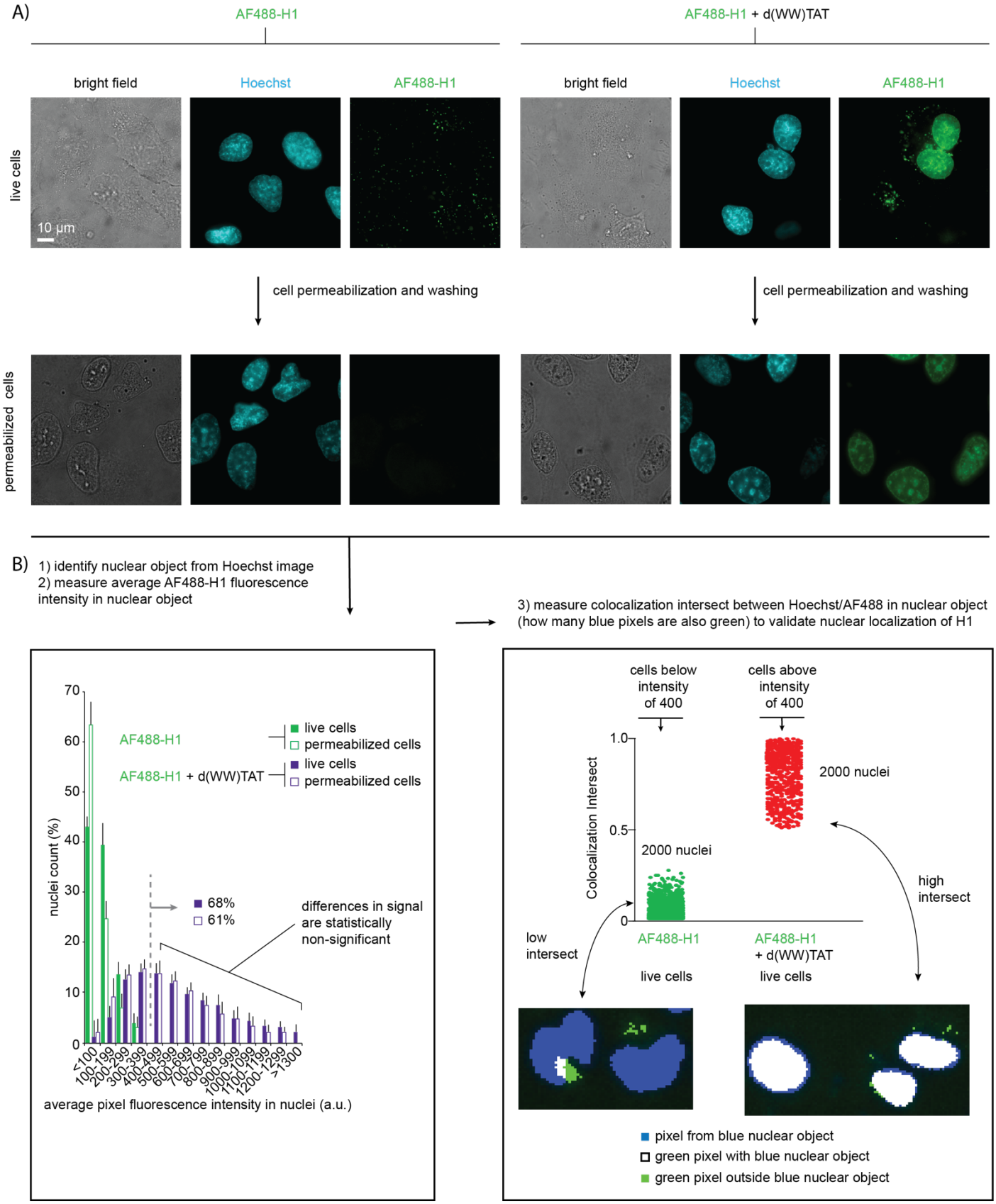
A)
AF488-H1
AF488-H1 + d(WW)TAT
bright field
Hoechst
AF488-H1
live cells
10 µm
cell permeabilization and washing
permeabilized cells
B)
1) identify nuclear object from Hoechst image
2) measure average AF488-H1 fluorescence intensity in nuclear object
3) measure colocalization intersect between Hoechst/AF488 in nuclear object (how many blue pixels are also green) to validate nuclear localization of H1
nuclei count (%)
AF488-H1
live cells
permeabilized cells
AF488-H1 + d(WW)TAT
68%
61%
differences in signal are statistically non-significant
average pixel fluorescence intensity in nuclei (a.u.)
cells below intensity of 400
cells above intensity of 400
Colocalization Intersect
2000 nuclei
high intersect
low intersect
pixel from blue nuclear object
green pixel with blue nuclear object
green pixel outside blue nuclear object

Figure S10. Extraction and analysis of nuclei containing AF488-H1. Scheme illustrating the general handling, nuclear extraction, and processing of Neuro2a cells incubated with AF488-H1 (0.75 μM) alone, or with AF488-H1 (0.75 μM) and d(WW)TAT (2.5 μM). A) Bright field and fluorescence images before and after permeabilization and washing of cytoplasmic components are provided. These nuclear isolation steps are performed while cells are still adhered to the plate (methods are described in Materials and Methods). Images are pseudocolored cyan for Hoechst and green for AF488-H1. The bright field imaging shows a drastic change in cell morphology, with nuclei being distinctively visible (the shape of the cells being discernable from what is likely cellular components adhering to the dish). Notably, fluorescent puncta corresponding to endosomal AF488-H1 is absent after this procedure, suggesting that endosomes are washed away after plasma membrane permeabilization and washing. There is also no detectable nuclear AF488-H1 signal in nuclei of the AF488-H1 alone conditions indicating that the green fluorescence signal detected in puncta in intact cells does not migrate to nuclei during the permeabilization/nuclear extraction protocol. B) Quantification of the nuclear AF488-H1 fluorescence intensity, before and after cell permeabilization. The nuclear intensities are processed as described in Figure S5, using Hoechst staining to identify nuclear objects (approximately 2500 cells are analyzed per condition). The AF488-H1 alone condition is used to establish a nuclear fluorescence threshold, with 99% of treated cells displaying a fluorescence signal below this threshold (indicated by the dashed line; herein the threshold intensity is 400). The number of nuclei displaying an intensity above this threshold in the AF488-H1+d(WW)TAT condition is quantified and indicated on the graph (the average and standard deviation of triplicate experiments are shown). The colocalization intersect, which measures the distribution of green pixels within the blue nuclear object, is used to confirm that the cells counted to have nuclear green intensities display a nuclear staining that is approximately matching the shape of the whole nucleus (as expected from H1 nuclear distribution. This is done to exclude the contribution of possible bright puncta in the vicinity of nuclei (as shown in the representative blue/green/white processed overlay images). Notably, the AF488-H1 nuclear intensities in the AF488-H1+d(WW)TAT condition are not statistically different before and after permeabilization/washing. Overall, based on microscopy imaging, we conclude that the nuclear extraction protocol does not lead to redistribution of AF488-H1 signal from endosomes to nuclei. Conversely, we conclude that permeabilization/washing does not cause a loss of nuclear signal, presumably because of strong retention of the histone protein by nuclear DNA. These results are further confirmed in Figure S11.

Figure S11

A)

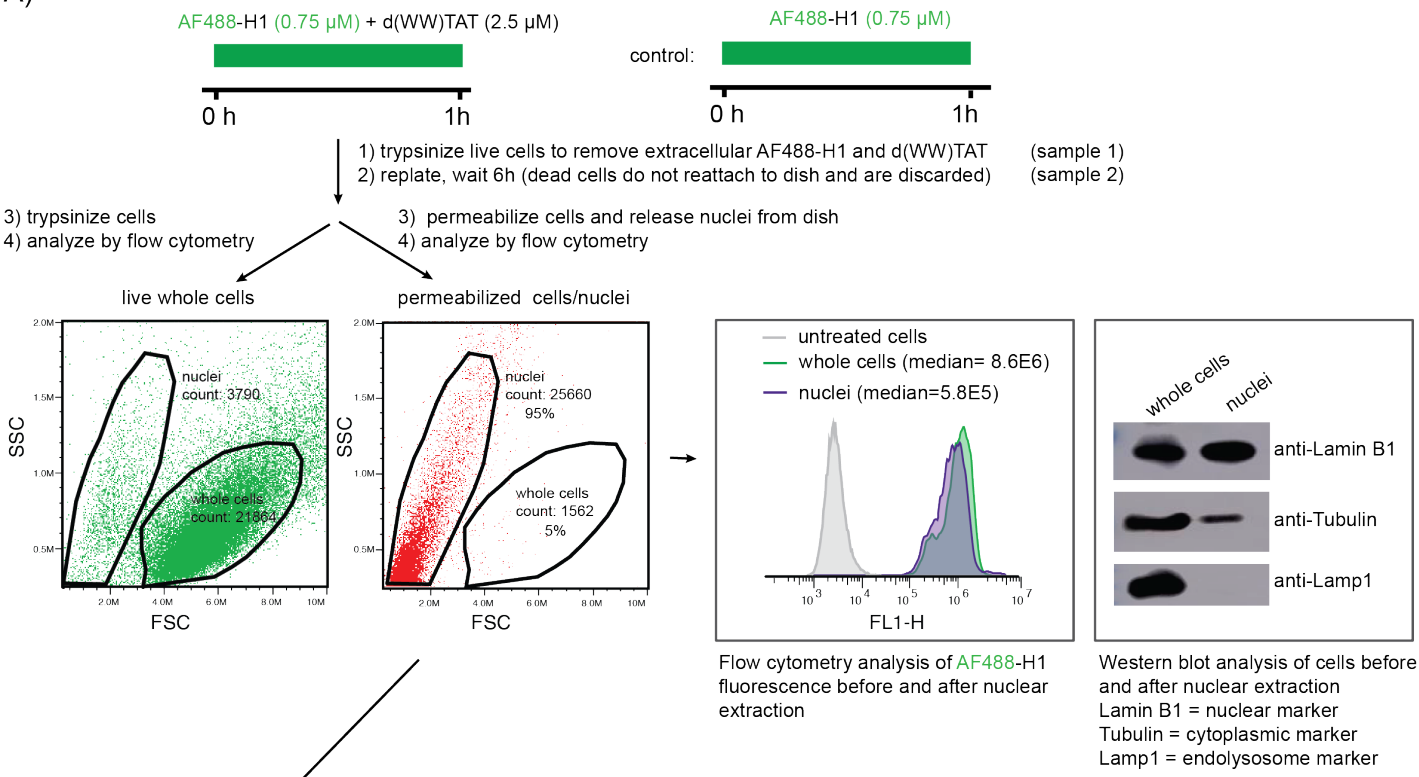

Flow cytometry analysis of AF488-H1 fluorescence before and after nuclear extraction

Western blot analysis of cells before and after nuclear extraction
Lamin B1 = nuclear marker
Tubulin = cytoplasmic marker
Lamp1 = endolysosome marker

B)

purification of extracted nuclei

use cell sorter on flow cytometer to collect nuclei based based on FSC,SSC, and Hoechst staining

sample 3

analyze on SDS-PAGE, using fluorescence scanner to detect AF488

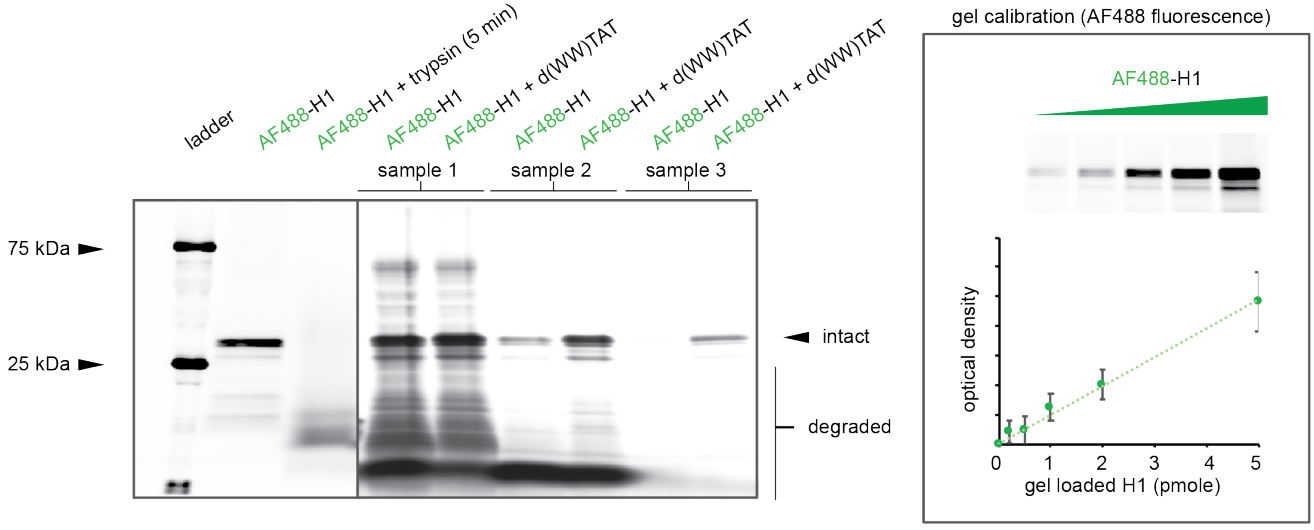

estimate: ~1.8 µM per nuclei
or ~400000 molecules per nuclei

Figure S11. AF488-H1 is intact and delivered into the nuclei of cells. A) Scheme describing the protocols used for the nuclear extraction process and the analysis of AF488-H1 in cell nuclei. Cells incubated for 1 h with AF488-H1 (0.75 μM) alone or with d(WW)TAT (2.5 μM) were washed with heparin and trypsinized to remove extracellular protein and peptide (sample 1) prior to transferring into a new dish. Cells, adherent after a 6 h incubation, were then permeabilized as in Figure S10 to recover all nuclei in solution. These nuclei were analyzed by western blotting (for presence of the nuclear marker lamin B1, and absence of the lysosomal marker Lamp1, along with tubulin as a cytoplasmic marker) and flow cytometry using side scattering (SSC) and forward scattering (FSC) (FSC intensity is proportional to the diameter of the object, SSC is dependent on internal components such as granules; Shapiro, Howard. Practical Flow Cytometry. New York, Alan R. Liss, 1985). Finally, the AF488-H1 signal (FL1-H) of cells was also analyzed by flow cytometry. Overall, these data are indicative of a nuclear extraction process that is 95% complete (i.e. 5% of cells keep SSC/FSC characteristics of whole cells) and that the nuclear extraction process leads to a loss in the AF488 signal from whole cells to nuclei (consistent with loss of cytoplasmic signal, and with possible loss from nuclear signal). B) Cells collected from samples 1 and 2, as well as nuclei sorted on a fluorescence-activated sorter (sample 3, nuclei are counted), were analyzed by SDS-PAGE, with detection of the AF488 signal using a fluorescence scanner. AF488-H1, before and after treatment with trypsin, was used as a loading control. Diluted samples from a stock of known concentration (obtained from lyophilized weighed protein) were used to establish a calibration curve. The AF488 intensity of gel bands was quantified by densitometry. The nuclei of cells incubated with AF488-H1 alone did not yield a detectable AF488-H1 signal. In contrast, a band with a molecular weight consistent to intact AF488-H1 was detected in the extracted nuclei of cells incubated with AF488-H1+d(WW)TAT. Densitometric analysis indicates that nuclei contain intact AF488-H1 at an estimated concentration of 1.8 μM per nuclei after delivery with d(WW)TAT. This estimate is in general agreement with results obtained in Figure S12 (where 3-10 μM concentrations are detected, a reduction in concentration being potentially accounted by the fact that cells were analyzed 6 h after delivery, and the fact that approximately 68% of nuclei in sample 3 are expected to contain H1, as described in Figure S10). Notably, cells incubated with AF488-H1 alone (sample 2) show more degraded fragments than cells incubated with AF488-H1+d(WW)TAT, and less intact H1 at the same time point. Based on fluorescence microscopy, this is consistent with AF488-H1 being exposed to proteases within the lumen of endosomes/lysosomes in the AF-488 H1 alone condition. Conversely, these results suggest that AF488-H1 is partially protected from degradation after delivery with d(WW)TAT. This is likely because the portion of AF488-H1 that reaches the nuclei is degraded less rapidly than the portion that remains trapped inside endosomes.

Figure S12

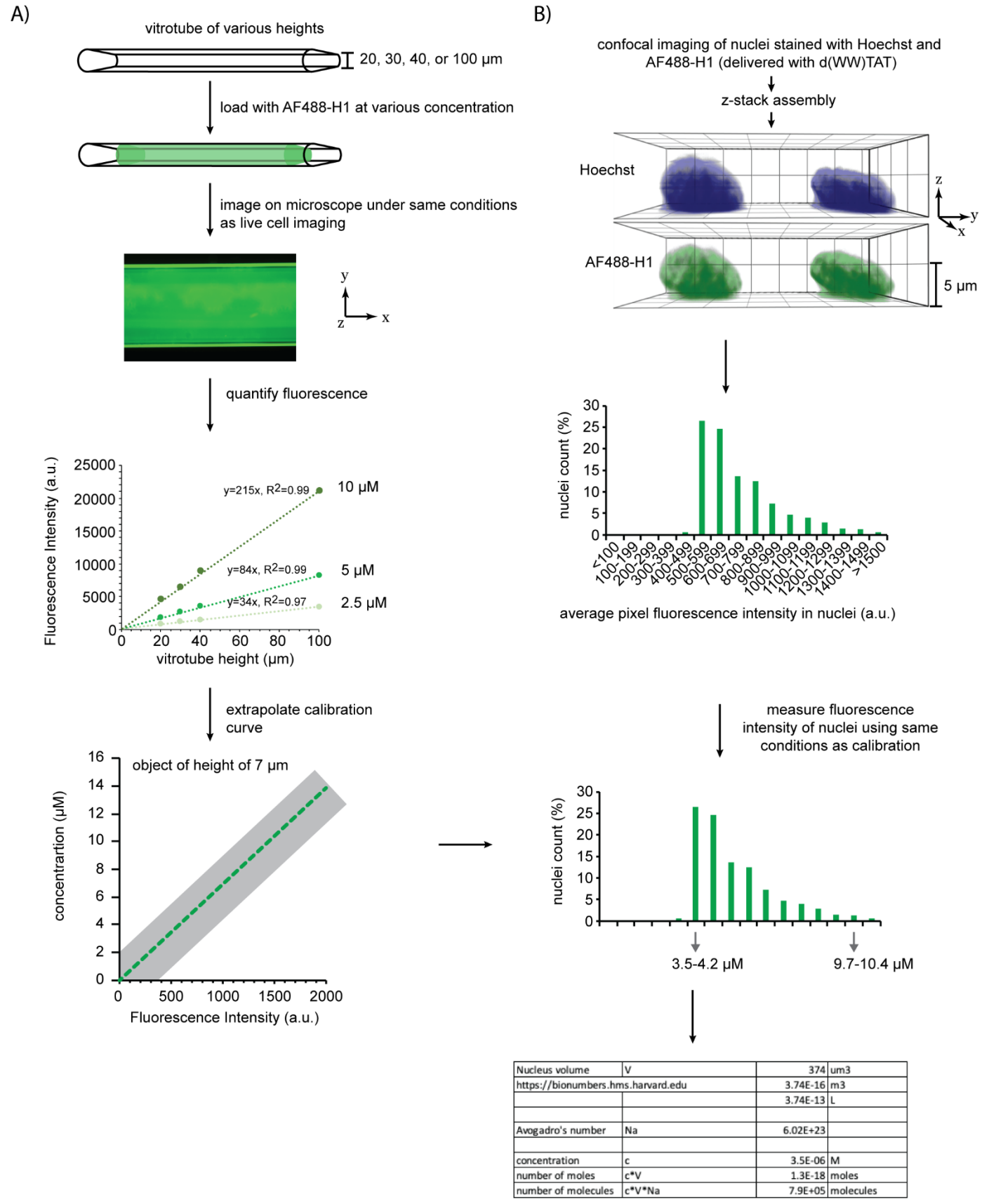

Nucleus volume	V	374	um3
https://bionumbers.hms.harvard.edu		3.74E-16	m3
		3.74E-13	L
Avogadro's number	Na	6.02E+23	
concentration	c	3.5E-06	M
number of moles	c*V	1.3E-18	moles
number of molecules	c*V*Na	7.9E+05	molecules

Figure S12. Estimate of the concentration of nuclear AF488-H1 after d(WW)TAT delivery by fluorescence microscopy. A) Calibration of the microscope with vitrotubes (VitroCom). Vitrotubes are flat miniature hollow glass capillary tubes with various heights (herein 20, 30, 40 and 100 µm, with a standard tolerance of 10%). Vitrotubes were filled with solutions of AF488-H1 of various concentrations and imaged by epifluorescence under conditions used for live cell imaging. The average pixel intensity obtained for each condition was quantified and used to establish a fluorescence intensity calibration curve for each sample depth (the contribution from out-of-focus fluorescence for each sample is correlated to the height (z-dimension) of the sample). In turn, a concentration/fluorescence intensity calibration curve is extrapolated for objects of a smaller height (herein, 7 µm, the average detected height of nuclei). The grey shading indicates the standard deviation obtained from 3 independent calibration experiments. B) HeLa cells incubated with AF488-H1 and d(WW)TAT were imaged by epifluorescence and confocal fluorescence microscopy (AF488-H1 is incubated at 0.75 µM for 1 h with 2.5 µM d(WW)TAT). 3D reconstruction of acquired z-stacks was used to estimate the height of the nuclear objects imaged (7 +/- 2 µm, 10 cells imaged). Epifluorescence images were then acquired, and the fluorescence intensities of nuclear objects were quantified (see Figure S10). The fluorescence intensities measured were compared to the calibration curves obtained with vitrotubes. This assay indicates that AF488-H1 nuclear concentrations detected are in the range of 3-10 µM. One caveat of this assay is that the nuclear height is outside the range measured with vitrotubes and could therefore be subject to different optical properties. Nonetheless, we present these data in combination with Figures S11 and S17 as validation that the nuclear intensities measured by different methods are consistent.

Figure S13

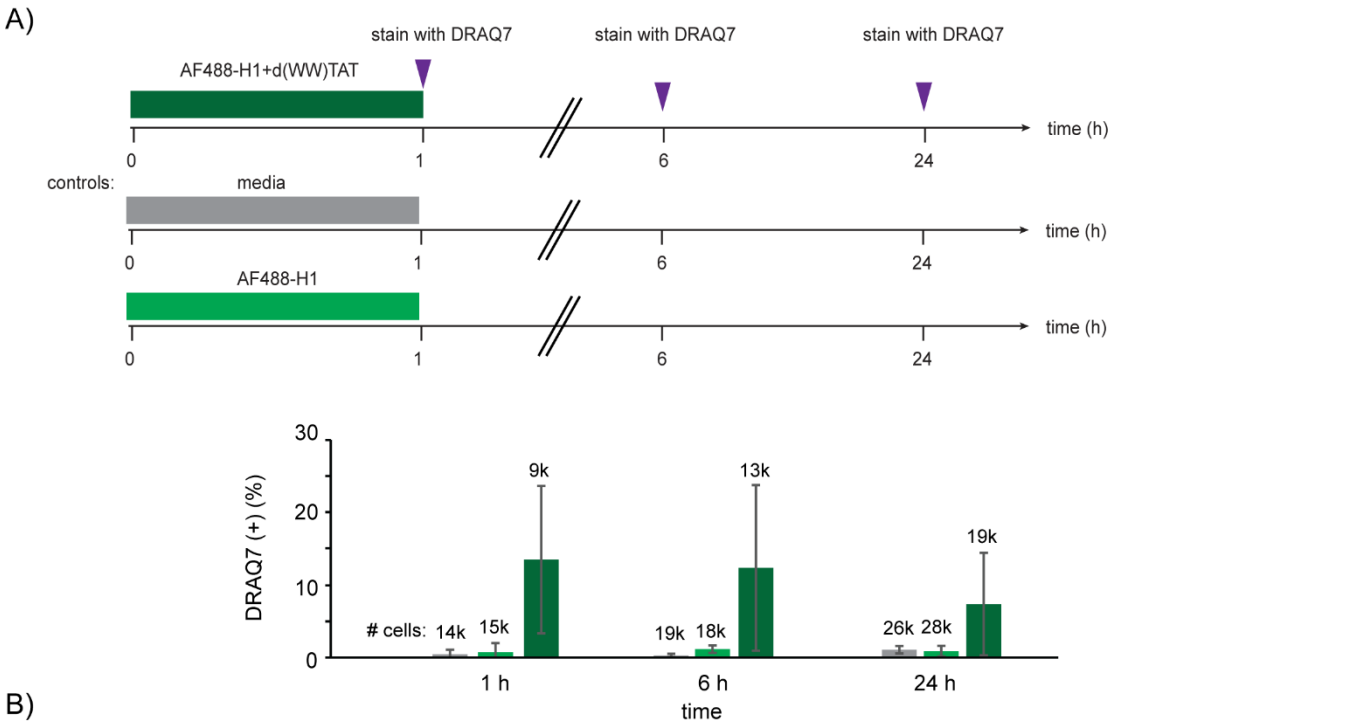
A)
stain with DRAQ7
stain with DRAQ7
stain with DRAQ7
AF488-H1+d(WW)TAT
time (h)
0
1
6
24
controls:
media
time (h)
AF488-H1
time (h)
DRAQ7 (+) (%)
30
20
10
0
cells:
14k
15k
9k
19k
18k
13k
26k
28k
19k
1 h
6 h
24 h
time

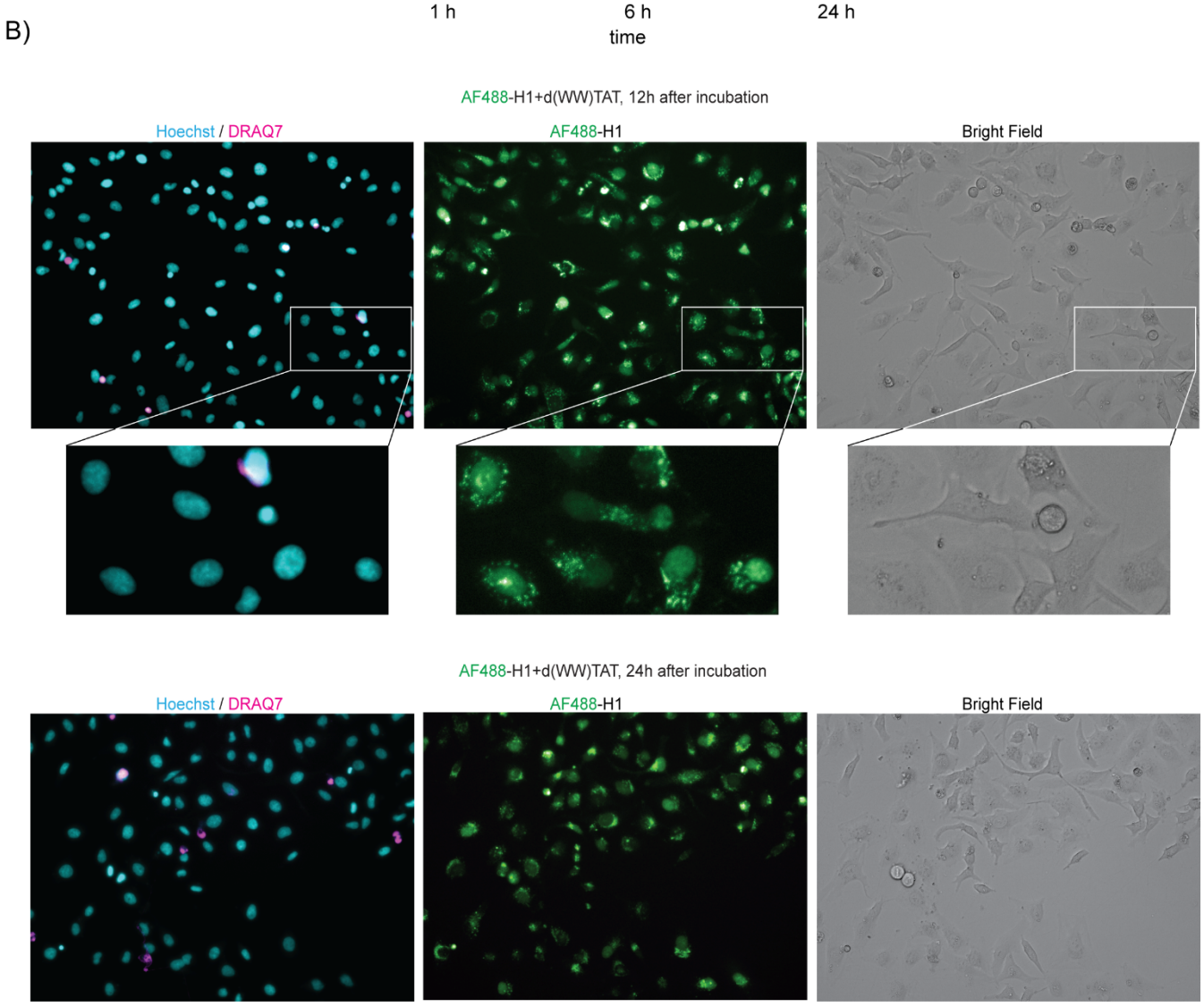
B)
AF488-H1+d(WW)TAT, 12h after incubation
Hoechst / DRAQ7
AF488-H1
Bright Field
AF488-H1+d(WW)TAT, 24h after incubation
Hoechst / DRAQ7
AF488-H1
Bright Field

Figure S13. Long term toxicity of HeLa following delivery of AF488-H1 with d(WW)TAT. The toxicity of d(X)TAT reagents reported in Figure 1 is measured 1 h after incubation (this time frame is generally sufficient to achieve cell delivery in a high percentage of cells, and from a delivery-protocol point of view, incubations for longer periods of time are not necessary). In turn, this raises the question of whether the cells that have been exposed to d(X)TAT and that are not detected as dead after incubation (as measured by SYTOX staining) would nonetheless be damaged and potentially die at later time points. To address this issue, cell death was monitored at 6 and 24 h post incubation with peptide. A) HeLa cells were treated with AF488-H1 (0.75 μM) alone or with d(WW)TAT (2.5 μM) for 1 h. Cells were then stained with DRAQ7 (a far-red fluorescent dye that stains dead cells with a permeabilized plasma membrane). Cells were imaged by fluorescence microscopy and analyzed by flow cytometry to count the number of DRAQ7 positive and DRAQ7 negative cells. Similar to Figure 1, the d(WW)TAT treatment leads to ~15% of DRAQ7 positive cells. Cells were then stained with DRAQ7 at 6 h or 24 h. Cells incubated with media alone or AF488-H1 alone were used as controls. The total number of cells in each sample is also indicated showing cell growth over the course of the experiment. B) Representative bright field and fluorescence microscopy images of HeLa treated with AF488-H1 and d(WW)TAT at 12 and 24 h time points. Zoom-in images are provided to highlight how nuclei remain stained with AF488-H1 at later time points.

Figure S14

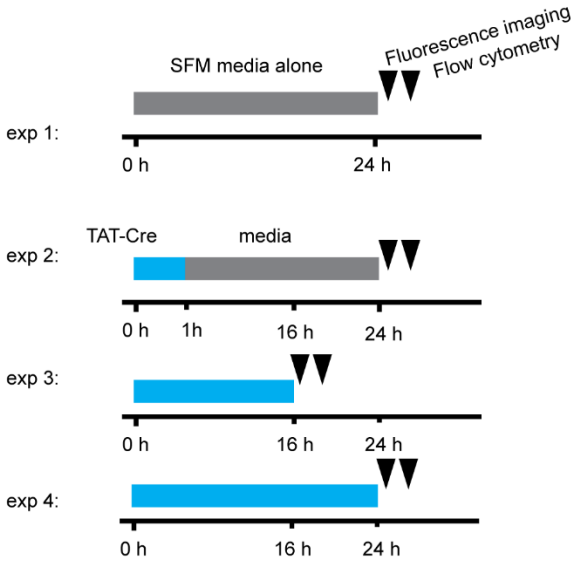

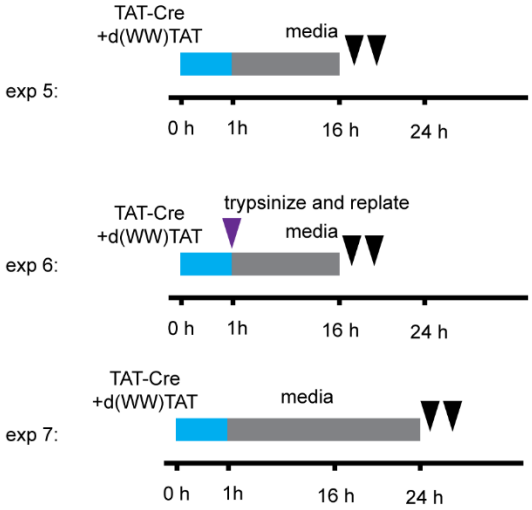

Fluorescence imaging:

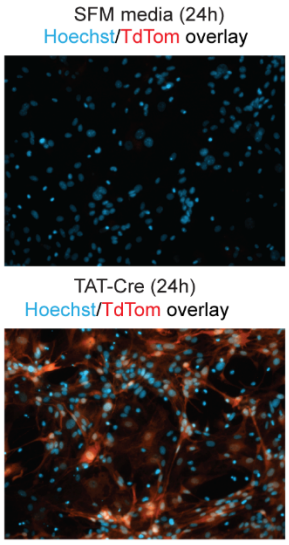

Flow cytometry:

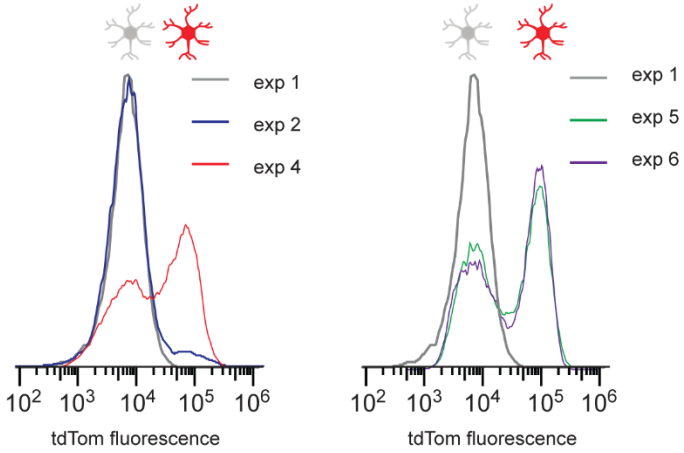

% tdTom(+):

exp 1: 0.1 % (gate at 99.9%)

exp 2: 4 +/- 2 %

exp 3: 8 +/- 6 %

exp 4: 35 +/- 12 %

exp 5: 53 +/- 3 %

exp 6: 55 +/- 5 %

exp 7: 58 +/- 6 %

Time course:

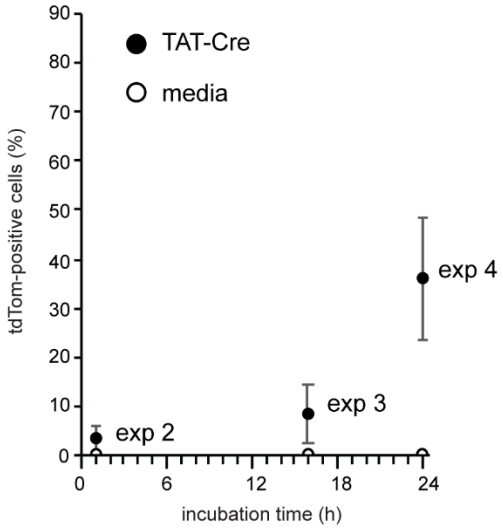

Figure S14. Comparison of TAT-Cre activity with and without peptide. Ai14 astrocytes were incubated with TAT-Cre (2 μM) alone for different lengths of time to measure the ability for TAT-Cre to induce gene recombination on its own (exp 1-4). Additionally, TAT-Cre was incubated with d(WW)TAT at 2.5 μM for 1 h and analyzed at both 16 and 24 h following incubation (exp 5 & 7). Finally, to measure the effect of extracellular TAT-Cre on recombination over time, a condition was included where cells were trypsinized following incubation to remove any TAT-Cre that was not taken up into astrocytes (exp 6). Analysis by flow cytometry shows that TAT-Cre is capable of inducing recombination without peptide present but requires a much longer incubation time than in the presence of d(WW)TAT. Extracellular TAT-Cre does not contribute to the percentage of cells undergoing recombination as no change was seen between trypsinized and non-trypsinized cells.

Figure S15

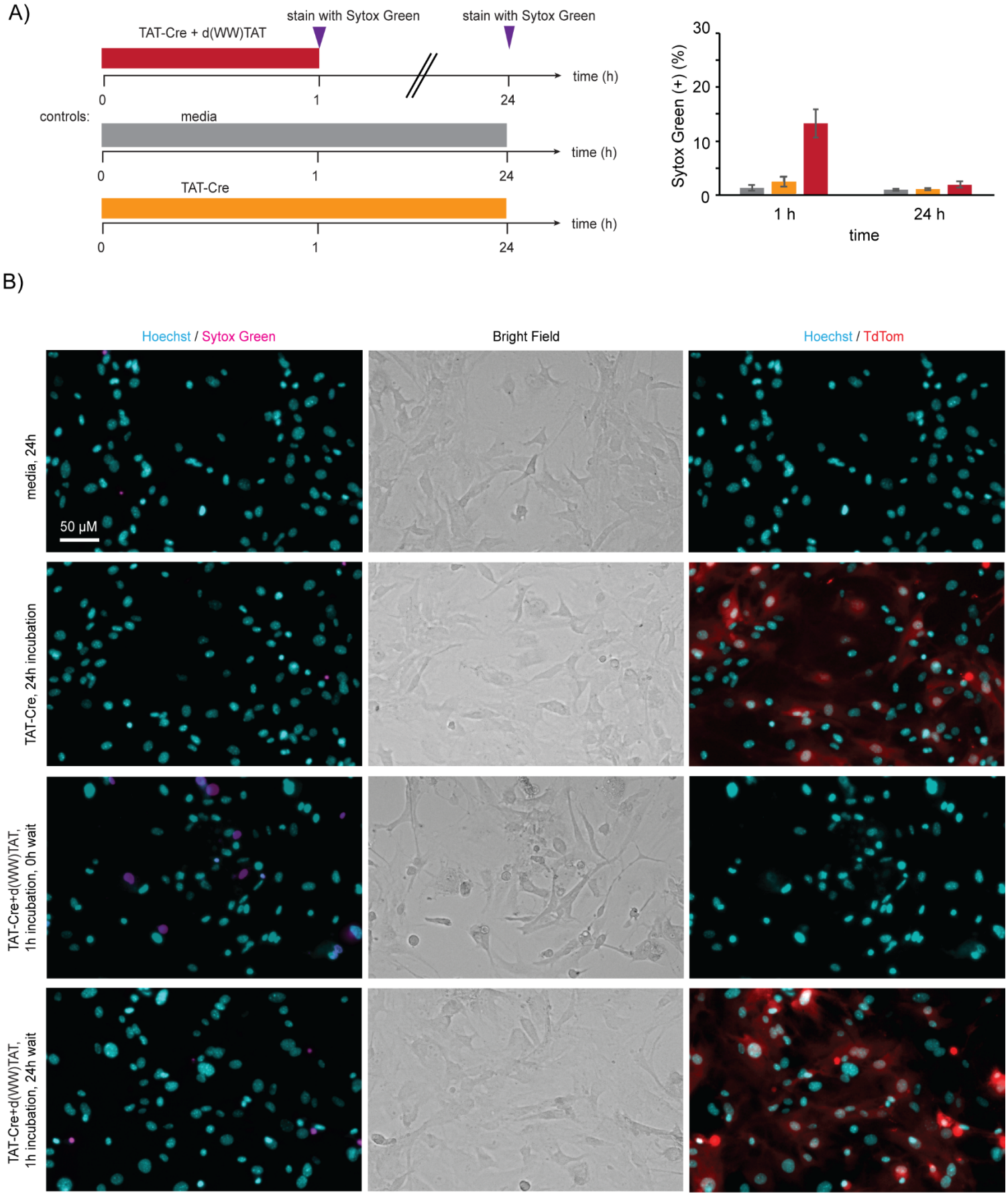
A)
stain with Sytox Green
stain with Sytox Green
TAT-Cre + d(WW)TAT
time (h)
0
1
24
controls:
media
time (h)
0
1
24
TAT-Cre
time (h)
0
1
24
Sytox Green (+) (%)
30
20
10
0
1 h
24 h
time
B)
Hoechst / Sytox Green
Bright Field
Hoechst / TdTom
media, 24h
50 µM
TAT-Cre, 24h incubation
TAT-Cre+d(WW)TAT, 1h incubation, 0h wait
TAT-Cre+d(WW)TAT, 1h incubation, 24h wait

Figure S15. Toxicity of Ai14 astrocytes over the course of 24 h after delivery of 2 μM TAT-Cre with 2.5 μM d(WW)TAT. Following delivery, approximately 15% of astrocytes displayed staining by SYTOX Green which is consistent with the toxicity expected for d(WW)TAT. Over the course of 24 hours the toxicity had returned to just above that expected for untreated astrocytes (~ 2%) which is likely due to dead cells detaching from the dish over the 24 h period.

Figure S16

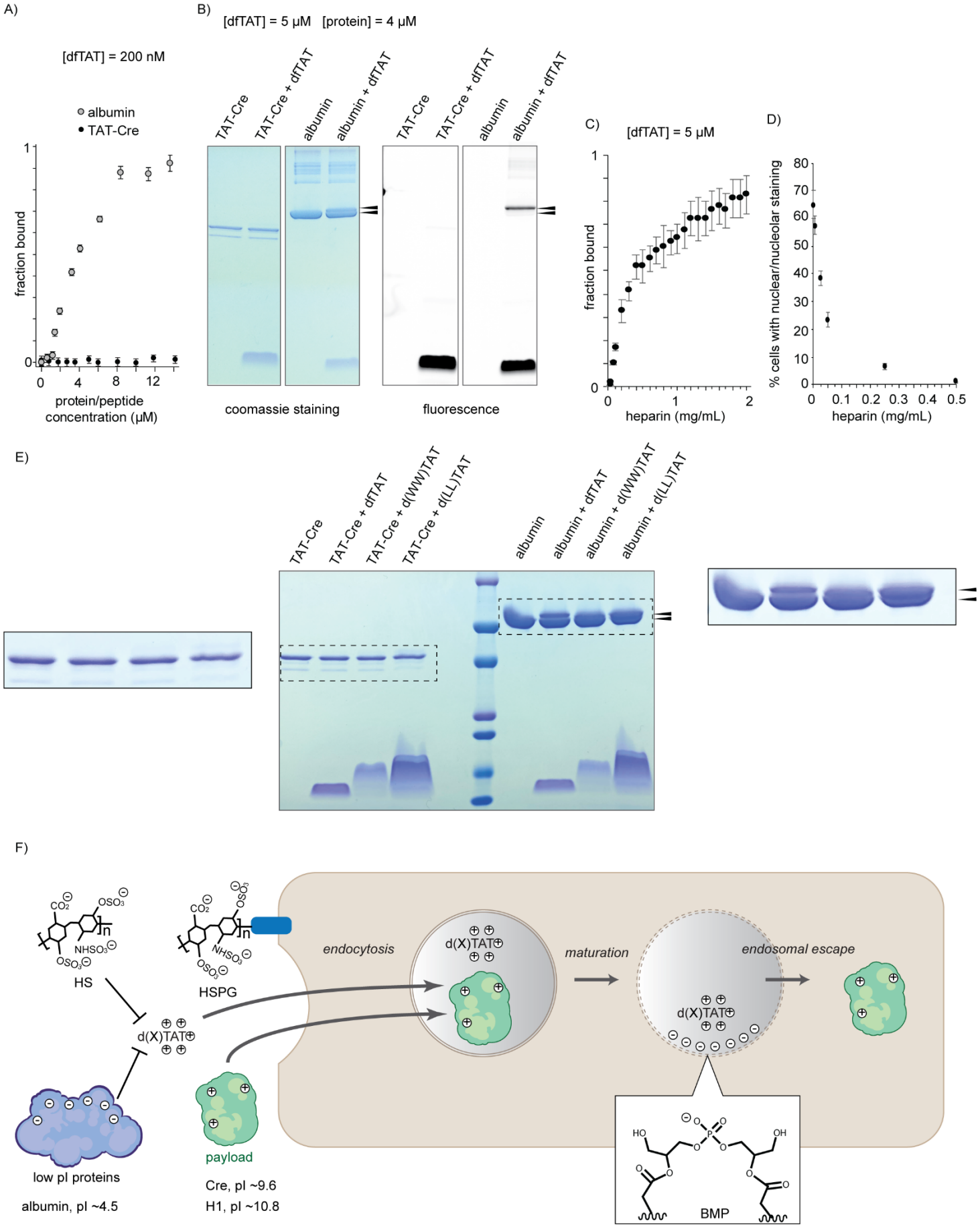
A)
[dfTAT] = 200 nM
albumin
TAT-Cre
fraction bound
protein/peptide concentration (μM)
B)
[dfTAT] = 5 μM [protein] = 4 μM
TAT-Cre
TAT-Cre + dfTAT
albumin
albumin + dfTAT
coomassie staining
fluorescence
C)
[dfTAT] = 5 μM
fraction bound
heparin (mg/mL)
D)
% cells with nuclear/nucleolar staining
heparin (mg/mL)
E)
TAT-Cre
TAT-Cre + dfTAT
TAT-Cre + d(WW)TAT
TAT-Cre + d(LL)TAT
albumin
albumin + dfTAT
albumin + d(WW)TAT
albumin + d(LL)TAT
F)
HS
HSPG
d(X)TAT
low pI proteins
albumin, pI ~4.5
payload
Cre, pI ~9.6
H1, pI ~10.8
endocytosis
maturation
endosomal escape
BMP

Figure S16. d(X)TAT binding and delivery. A) Binding of dfTAT to TAT-Cre as evaluated by fluorescence anisotropy. Bovine albumin is used as a control. dfTAT was diluted in L15 to a concentration of 200 nM. The binding of dfTAT to proteins was determined by titrating the proteins and determining the change of the fluorescence anisotropy for different total protein concentrations. The average fraction bound determine from triplicate is reported. B) Native gel electrophoresis of solutions containing mixtures of TAT-Cre and dfTAT or albumin and dfTAT. Gels were imaged with a fluorescence scanner to detect the TMR signal of dfTAT, and subsequently stained with Coomassie. C) Binding of dfTAT to heparin measured by fluorescence anisotropy. D) Effect of extracellularly administered heparin on the intracellular entry of dfTAT. dfTAT was incubated with HeLa cells at 5 μM for 1h in the presence of various amount of heparin. Intracellular access was assessed by measuring the nuclear/nucleolar staining of the peptide by fluorescence microscopy, as described in Figure 1). E) SDS-PAGE highlighting the binding of dfTAT, d(WW)TAT and d(LL)TAT to BSA but not TAT-Cre. F) Model describing how electrostatic interactions between d(X)TAT and extracellular anionic species may inhibit cell delivery.

Figure S17

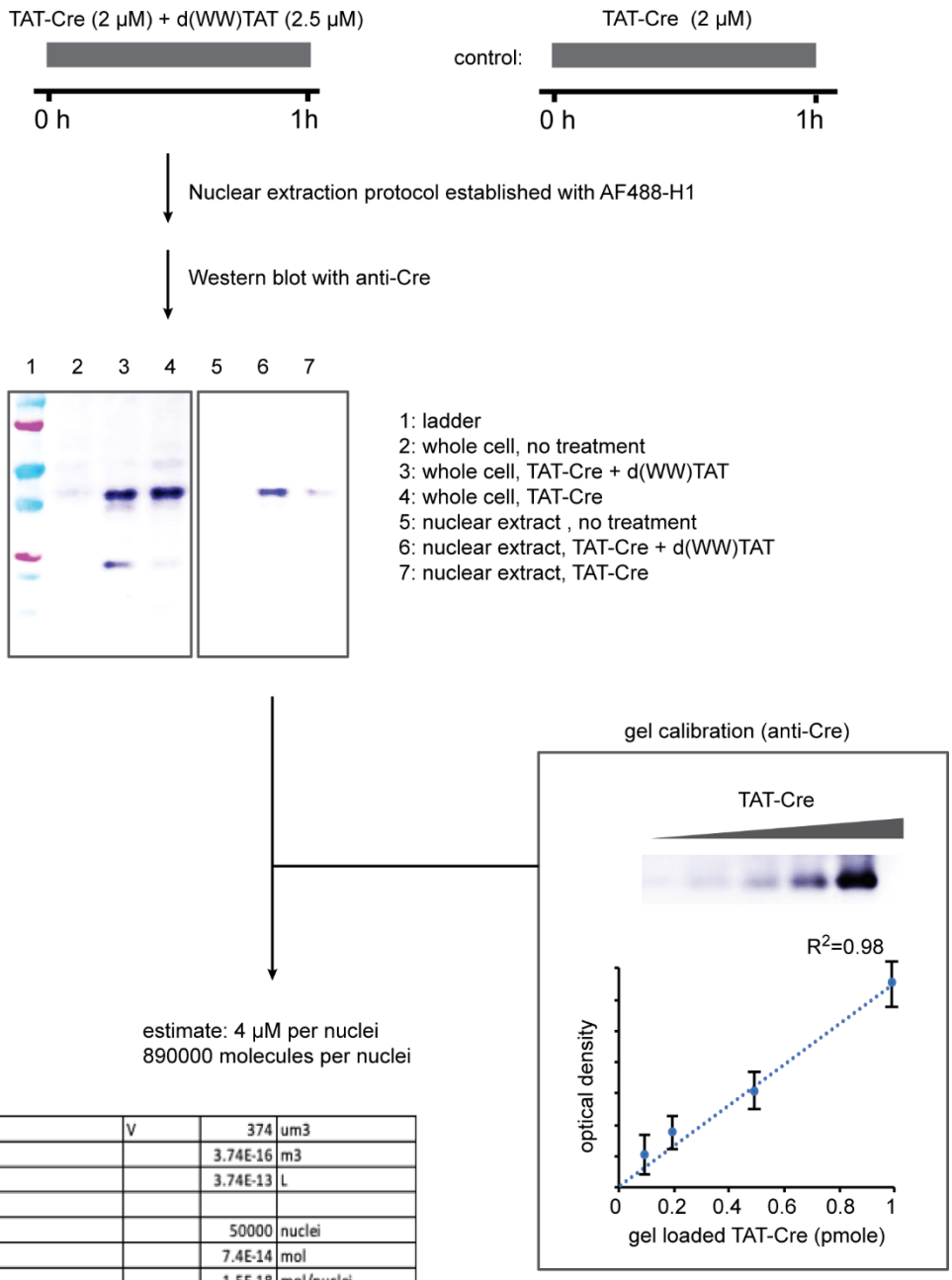

Nucleus volume	V	374	um3
https://bionumbers.hms.harvard.edu		3.74E-16	m3
		3.74E-13	L
nuclei		50000	nuclei
number of moles		7.4E-14	mol
number of moles per nuclei		1.5E-18	mol/nuclei
Avogadro's number	Na	6.02E+23	/mol

Figure S17. Quantitation of intact TAT-Cre that reaches the nucleus following delivery by d(WW)TAT. After delivery of TAT-Cre (2 μM) with d(WW)TAT (2.5 μM) for 1h, whole cell samples were collected and nuclei were extracted following the protocol established in Figure S11 (the same controls were used to assess the purity of the extracted nuclei). Western blotting analysis of the samples was performed using an anti-Cre monoclonal antibody. Based on this analysis, TAT-Cre is detected in relatively equal quantities in whole cell lysates, with or without d(WW)TAT (this is consistent with the notion that TAT-Cre is endocytosed by cells whether d(WW)TAT is present or not). However, in the presence of d(WW)TAT, TAT-Cre localizes in nuclei. In contrast, only a weak signal is detected when d(WW)TAT is not present. Comparison of this TAT-Cre signal to a calibration curve of TAT-Cre indicates a nuclear concentration of ~4 μM for TAT-Cre.

Figure S18

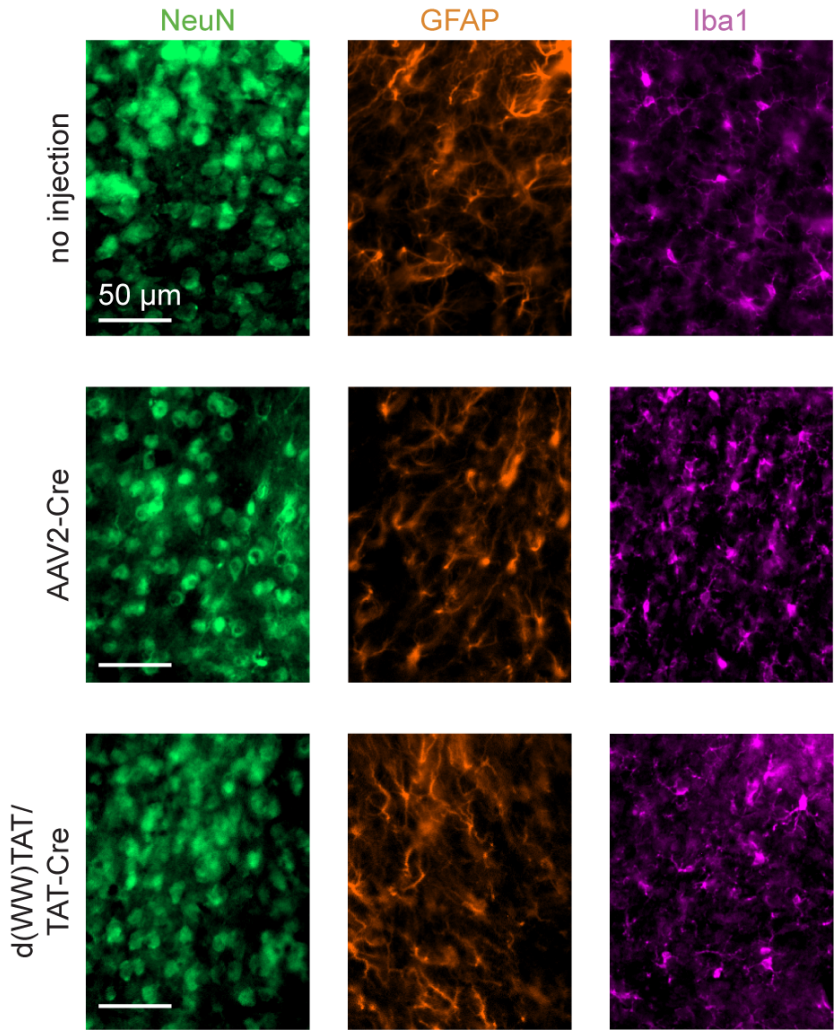

Figure S18. Representative images from quantified brain slices. Representative images from regions where the neuron (NeuN), astrocyte (GFAP), and microglia (Iba1) cell densities were quantified in Figure 3C.

Figure S19

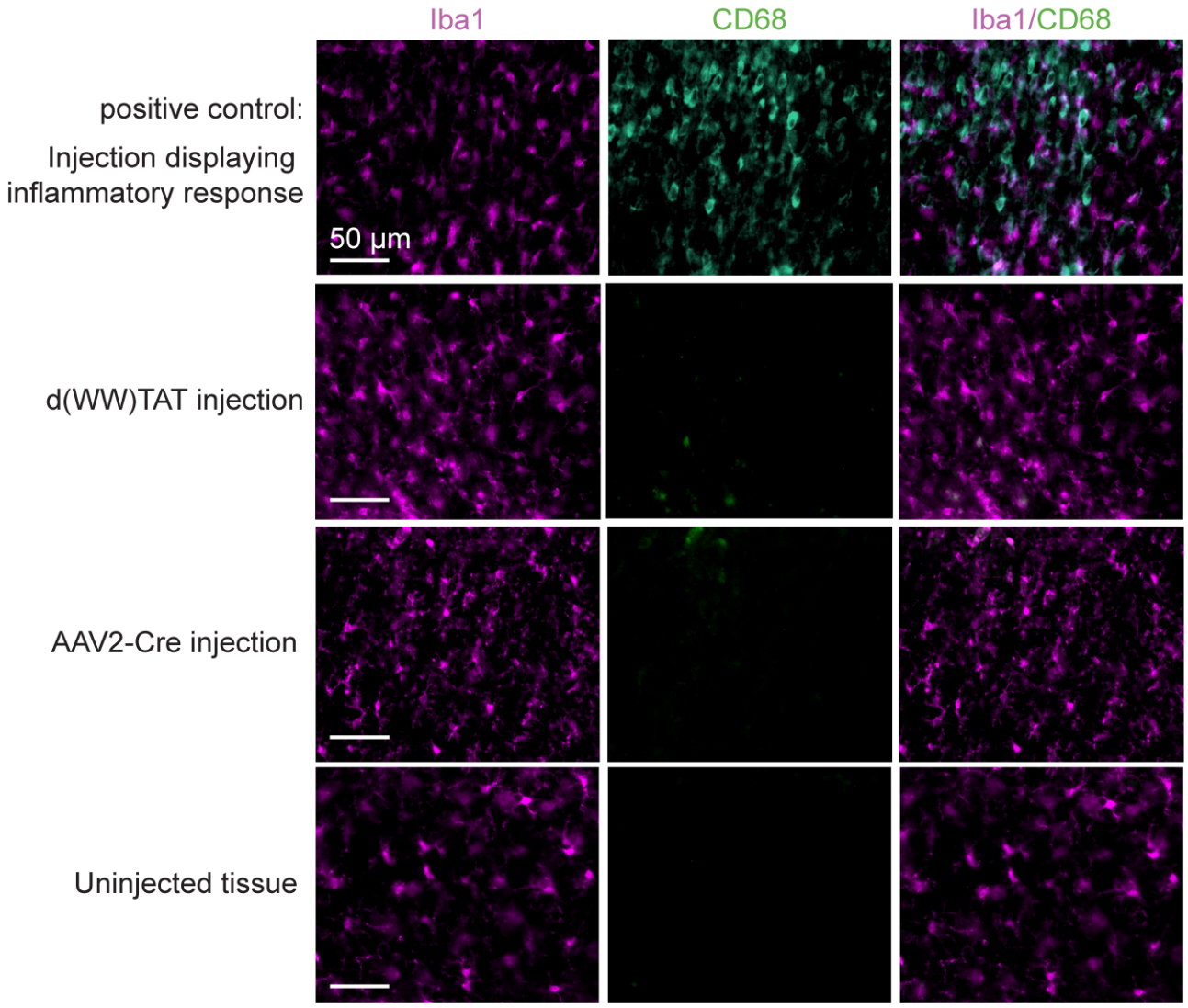

Figure S19. Representative images of inflammatory response in the brain. Representative images of inflammatory response at different injections based on CD68 stain. A positive control is included (top images) to confirm the stain does bind in areas where there is damage.

Figure S20

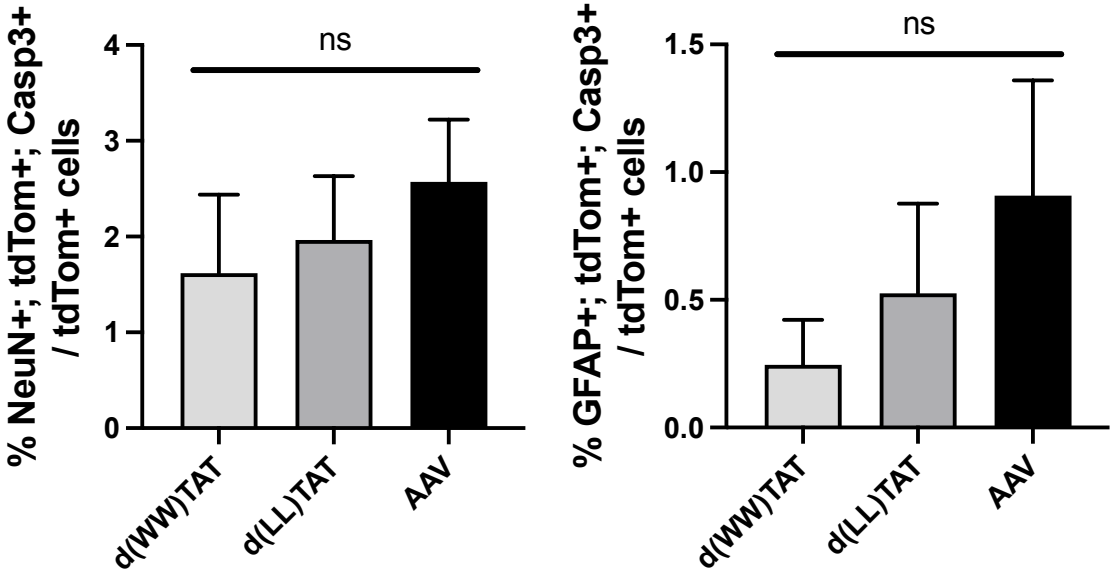

Figure S20. Cleaved Caspase3 Immunohistochemistry. The tissue processed for immunohistochemistry 14 days after cortical injection of peptide/cargo or AAV-Cre (see main methods) was stained for cleaved caspase 3 to assess apoptosis caused by the injections. Brain sections were co-stained for cleaved caspase 3 (marker for apoptotic cells), NeuN (marker for neurons) and GFAP (marker for astrocytes) as these were the primary cell types expressing tdTom-induced by Cre delivery. At 14-days post-injection, there was a small number of cleaved caspase 3-expressing cells in all sections, mostly around the AAV-Cre and the peptide injection sites. Quantification of the number of cleaved caspase 3 and tdTom expression in the neuronal or astrocytic population show there is no significant difference in apoptosis induced by cortical injections of peptide/cargo or AAV-Cre, suggesting that the delivery of the peptide/cargo does not induce apoptosis.

Figure S21

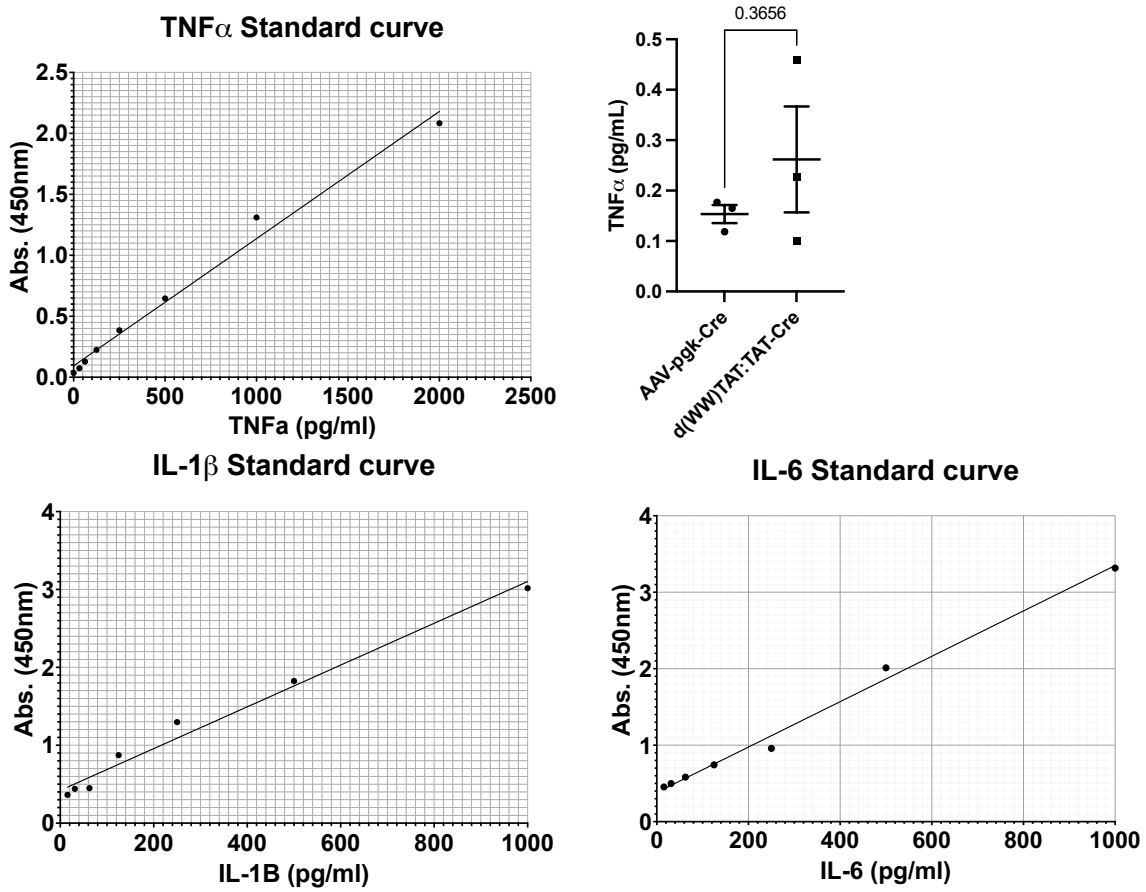

Figure S21. Pro-inflammatory Cytokine ELISA for Acute Inflammatory Response. 10 weeks old male Ai14 were injected with either d(WW)TAT:TAT-Cre (N=3) or AAV-Cre (N=3) bilaterally in the cortex, and solid-phase sandwich ELISAs were performed to asses inflammatory cytokines TNF-α, IL-1β and IL-6 at the injection site 3-days post-injection. The levels of both IL-1β and IL-6 were below the level detectable by this assay when the samples were run at a total protein concentration of 10µg/mL suggesting no increase in inflammation in the d(WW)TAT:TAT-Cre injection sites compared to the AAV-Cre. TNF-α levels were measurable but below 1pg/mL in all the samples, both peptide and AAV injected. There was non-significant difference in the TNF-α levels in the d(WW)TAT:TAT-Cre injection sites compared to the AAV-Cre.

Figure S20

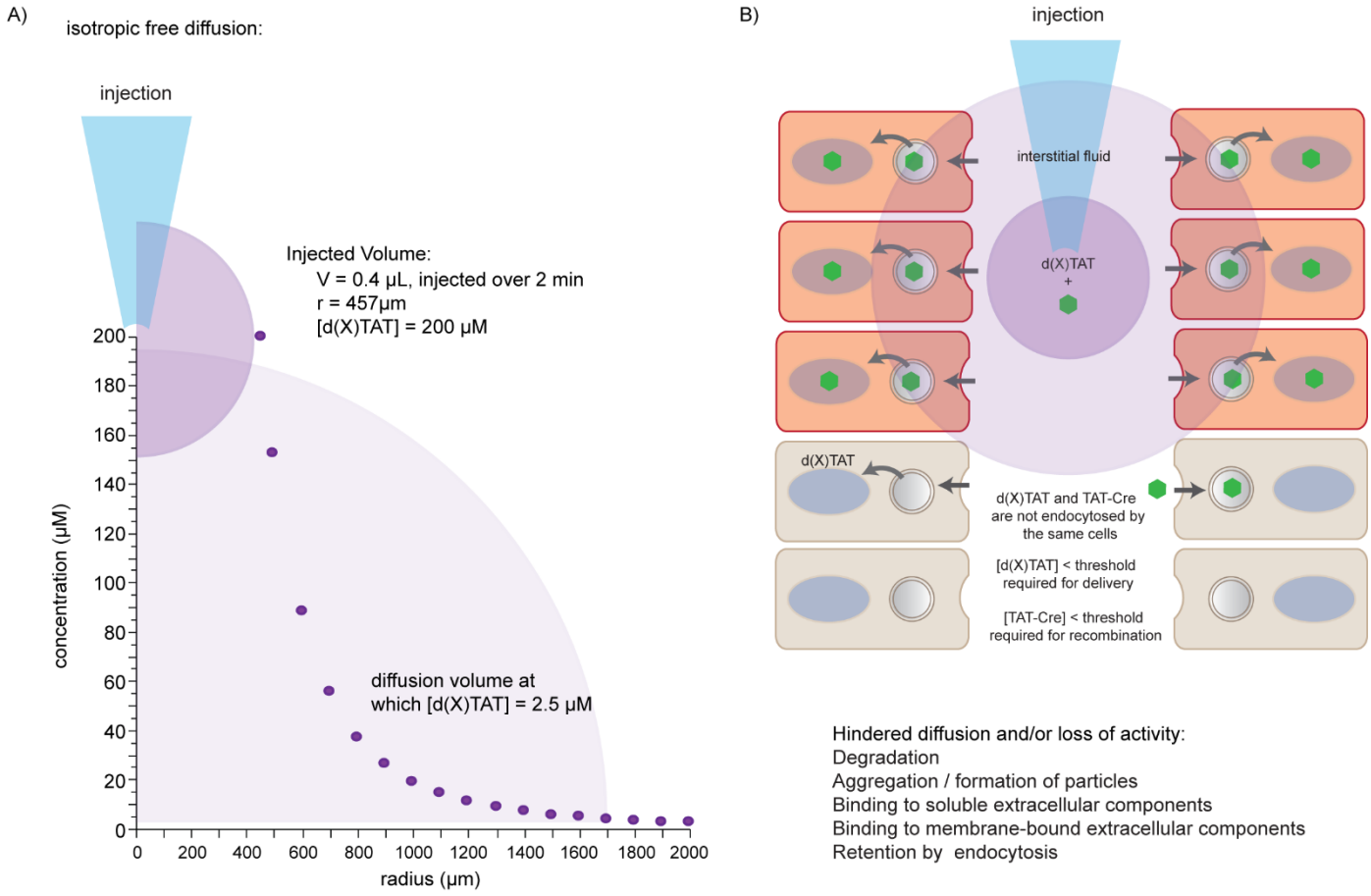

Figure S22. *In vivo* diffusion radius. A) Model for the dilution of d(X)TAT upon *in vivo* injection. This model assumes an isotropic free diffusion of the molecules and shows the dependence of the peptide concentration on the diffusion radius (assuming diffusion in a sphere of increasing radius r with a volume of 4/3 πr^3). B) Model highlighting examples of factors that could limit the diffusion of d(X)TAT.

Figure S23

A)

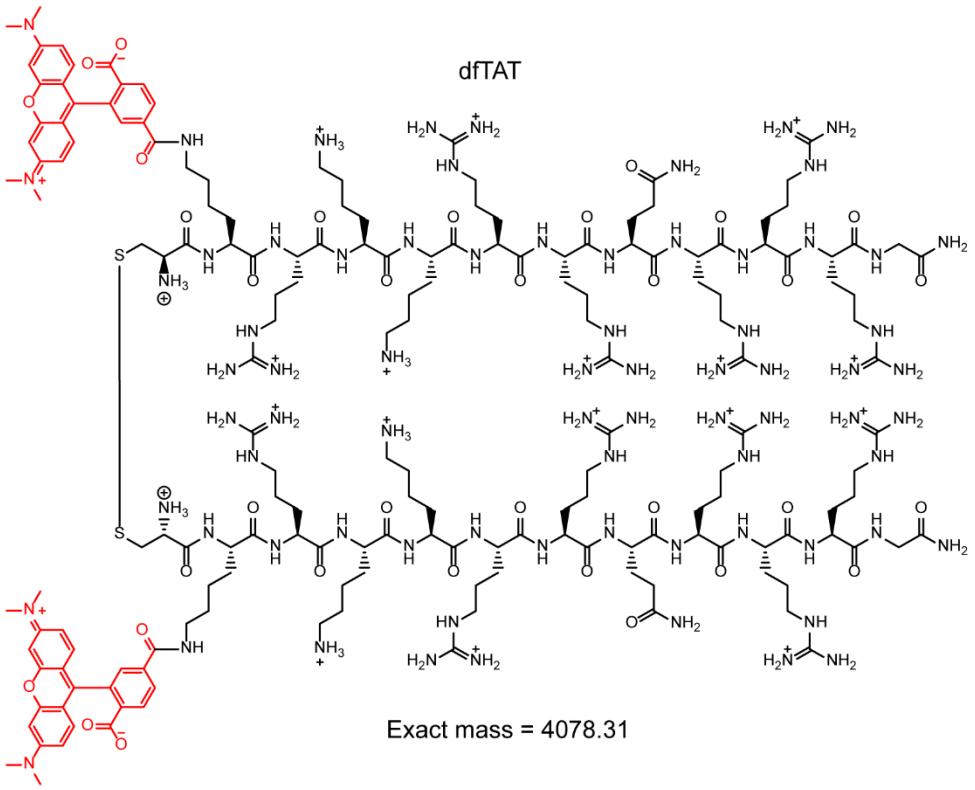

B)

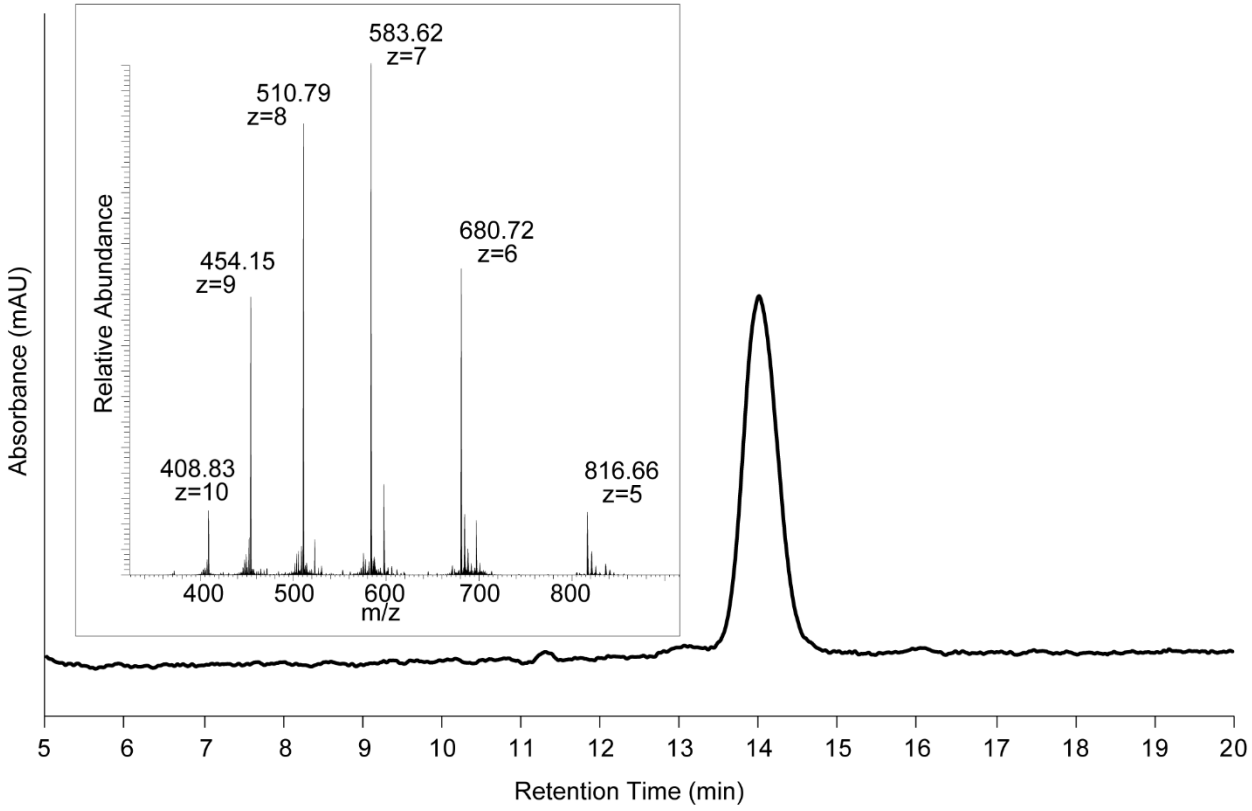

Figure S24

A)

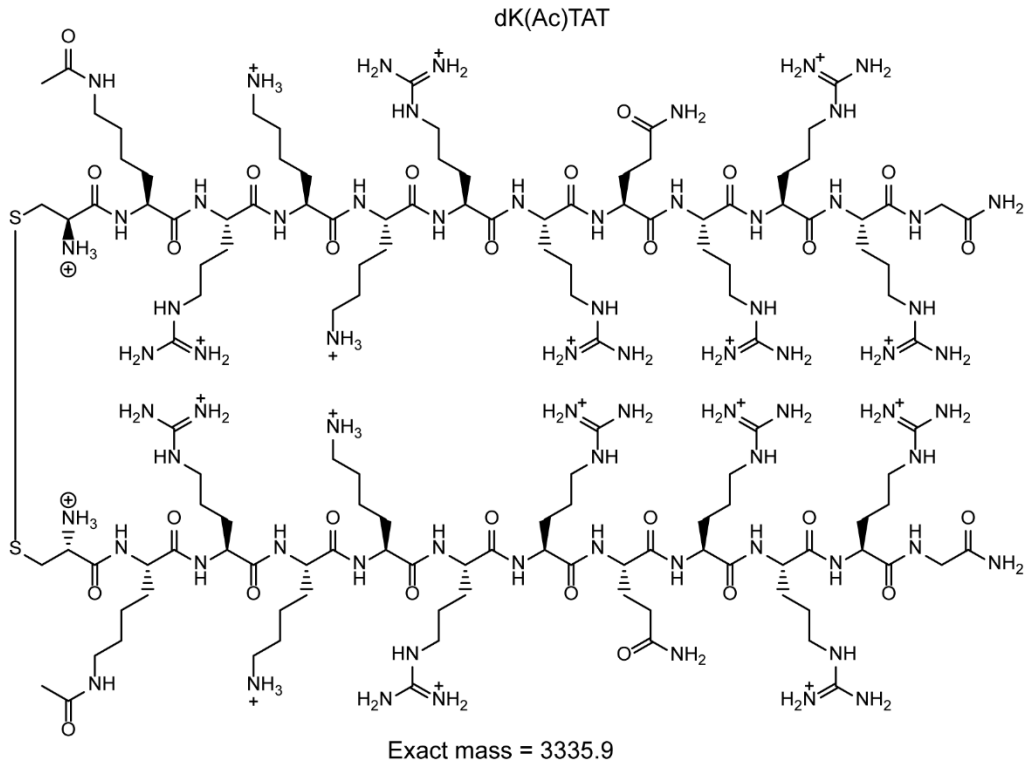

B)

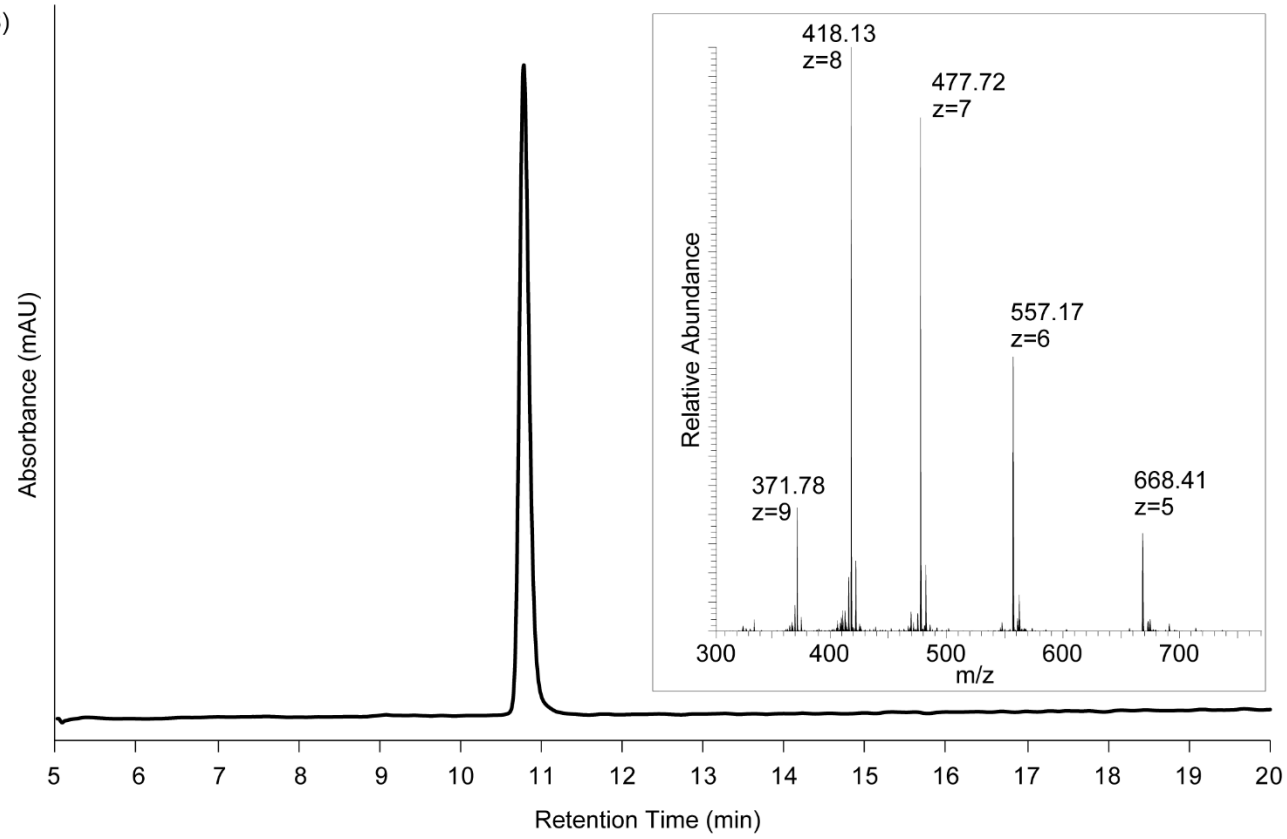

Figure S25

A)

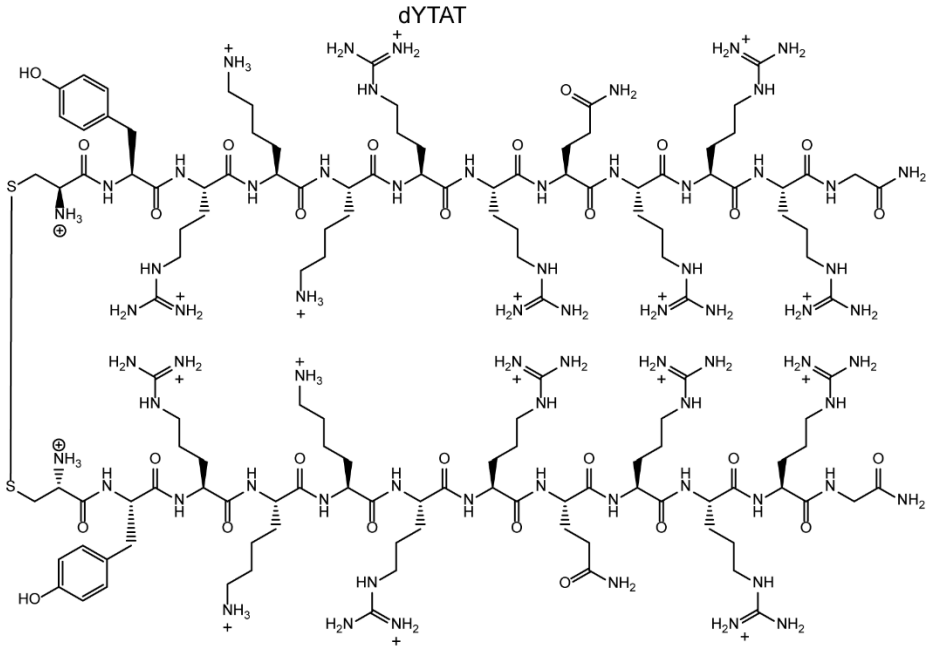

Exact mass = 3322.01

B)

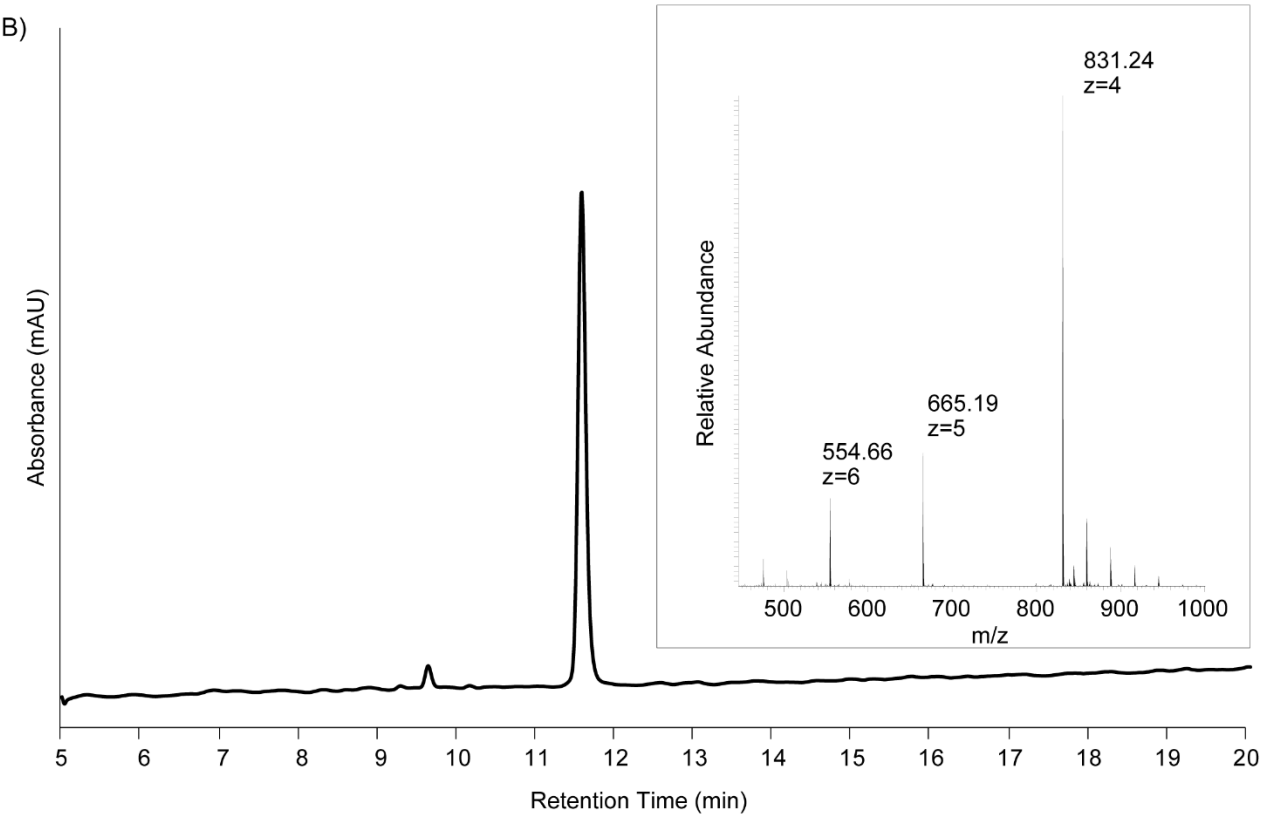

Figure S26

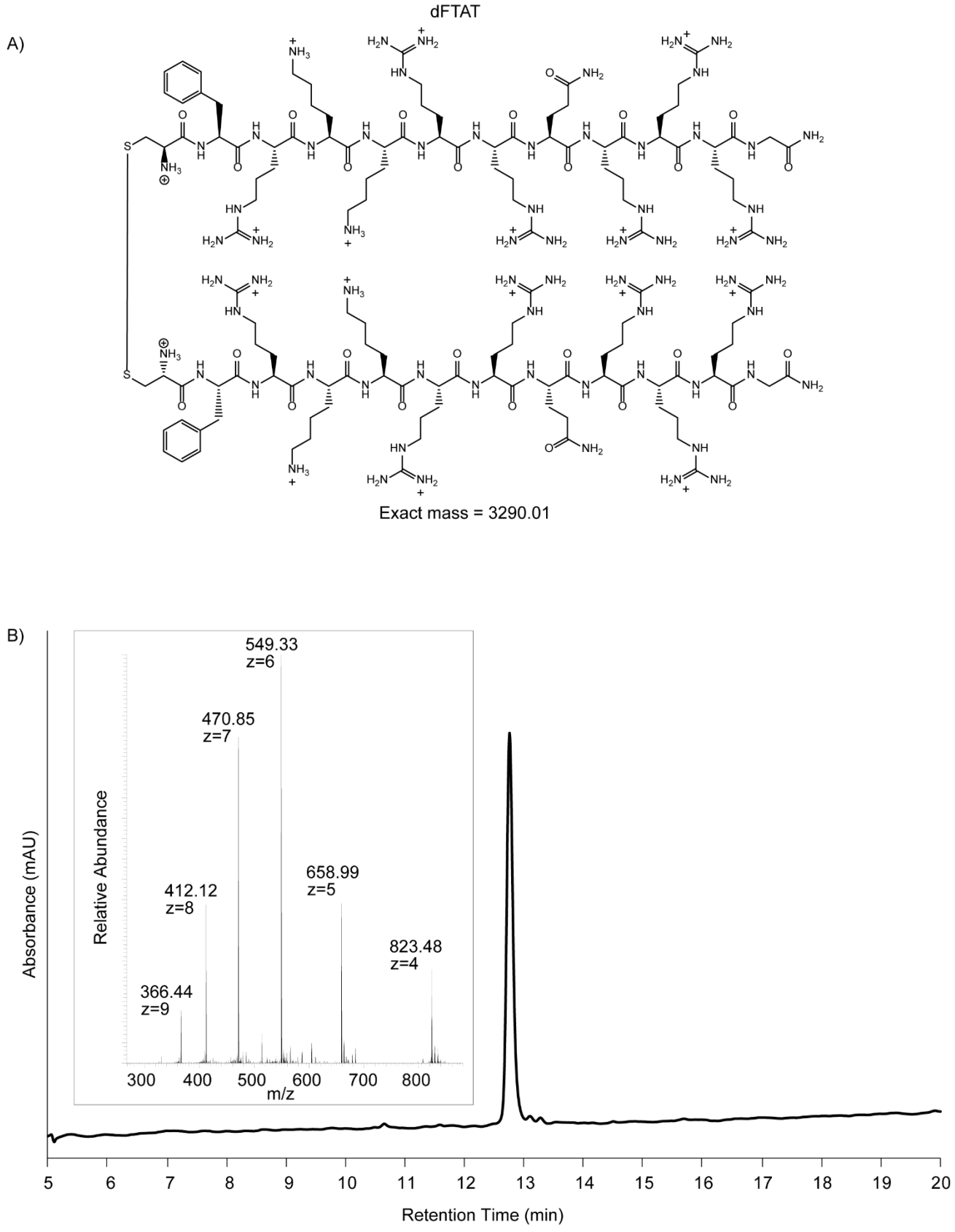
A)
dFTAT
Exact mass = 3290.01
B)
549.33
z=6
470.85
z=7
412.12
z=8
658.99
z=5
823.48
z=4
366.44
z=9
Relative Abundance
m/z
300
400
500
600
700
800
Absorbance (mAU)
Retention Time (min)
5
6
7
8
9
10
11
12
13
14
15
16
17
18
19
20

Figure S27

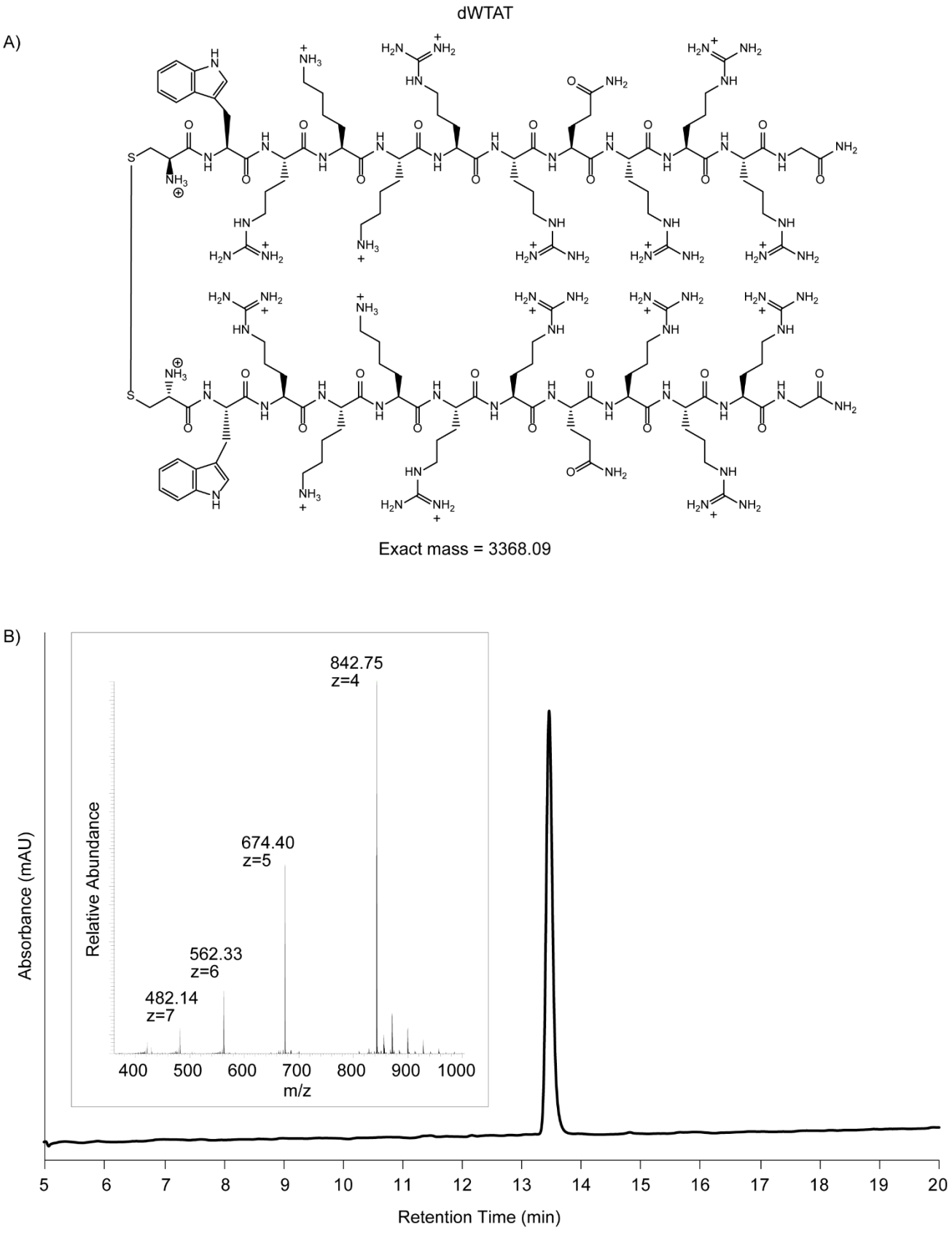
dWTAT
A)
Exact mass = 3368.09
B)
842.75
z=4
674.40
z=5
562.33
z=6
482.14
z=7
Relative Abundance
m/z
400
500
600
700
800
900
1000
Absorbance (mAU)
Retention Time (min)
5
6
7
8
9
10
11
12
13
14
15
16
17
18
19
20

Figure S28

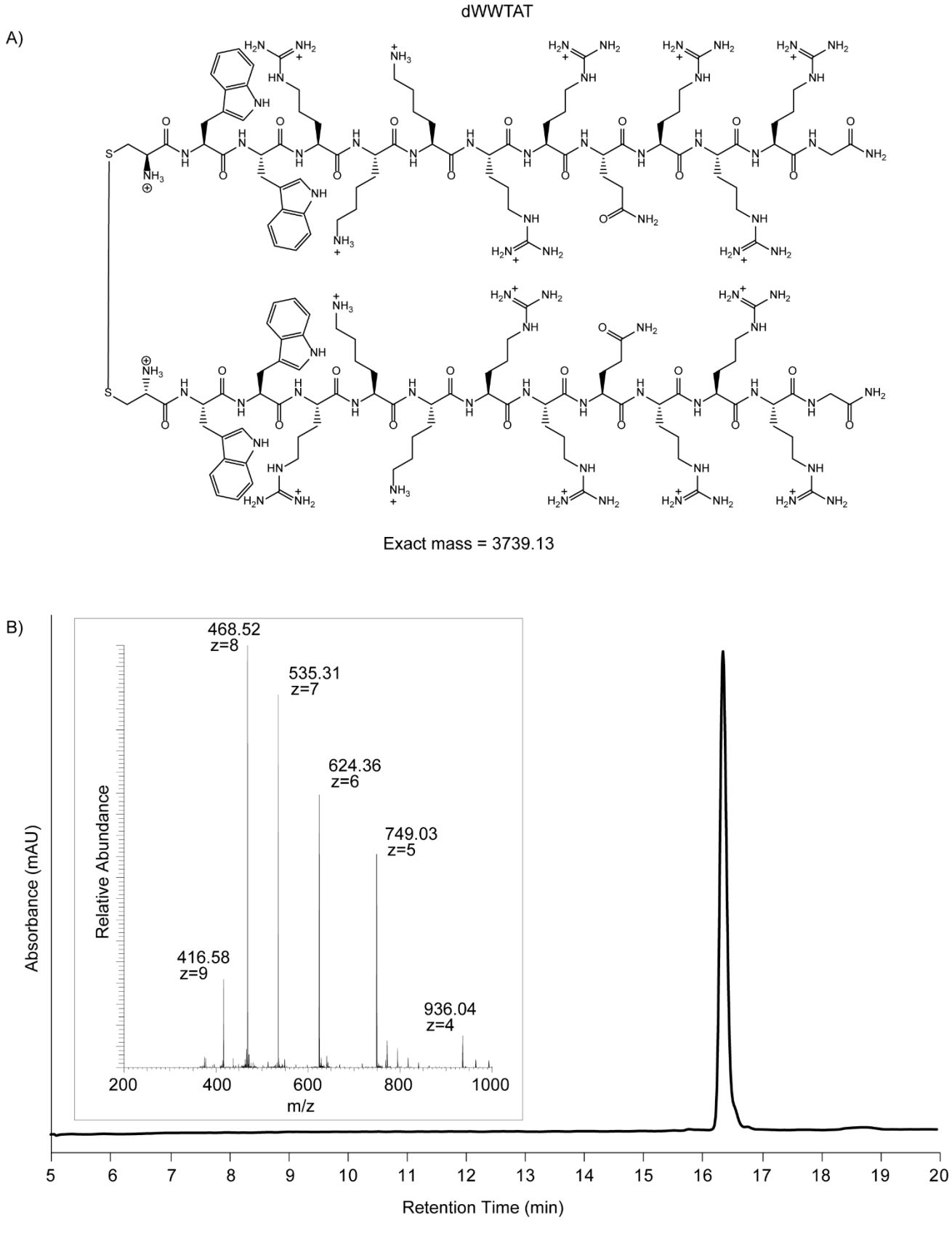
dWWTAT
A)
Exact mass = 3739.13
B)
468.52
z=8
535.31
z=7
624.36
z=6
749.03
z=5
416.58
z=9
936.04
z=4
Relative Abundance
m/z
200
400
600
800
1000
Absorbance (mAU)
Retention Time (min)
5
6
7
8
9
10
11
12
13
14
15
16
17
18
19
20

Figure S29

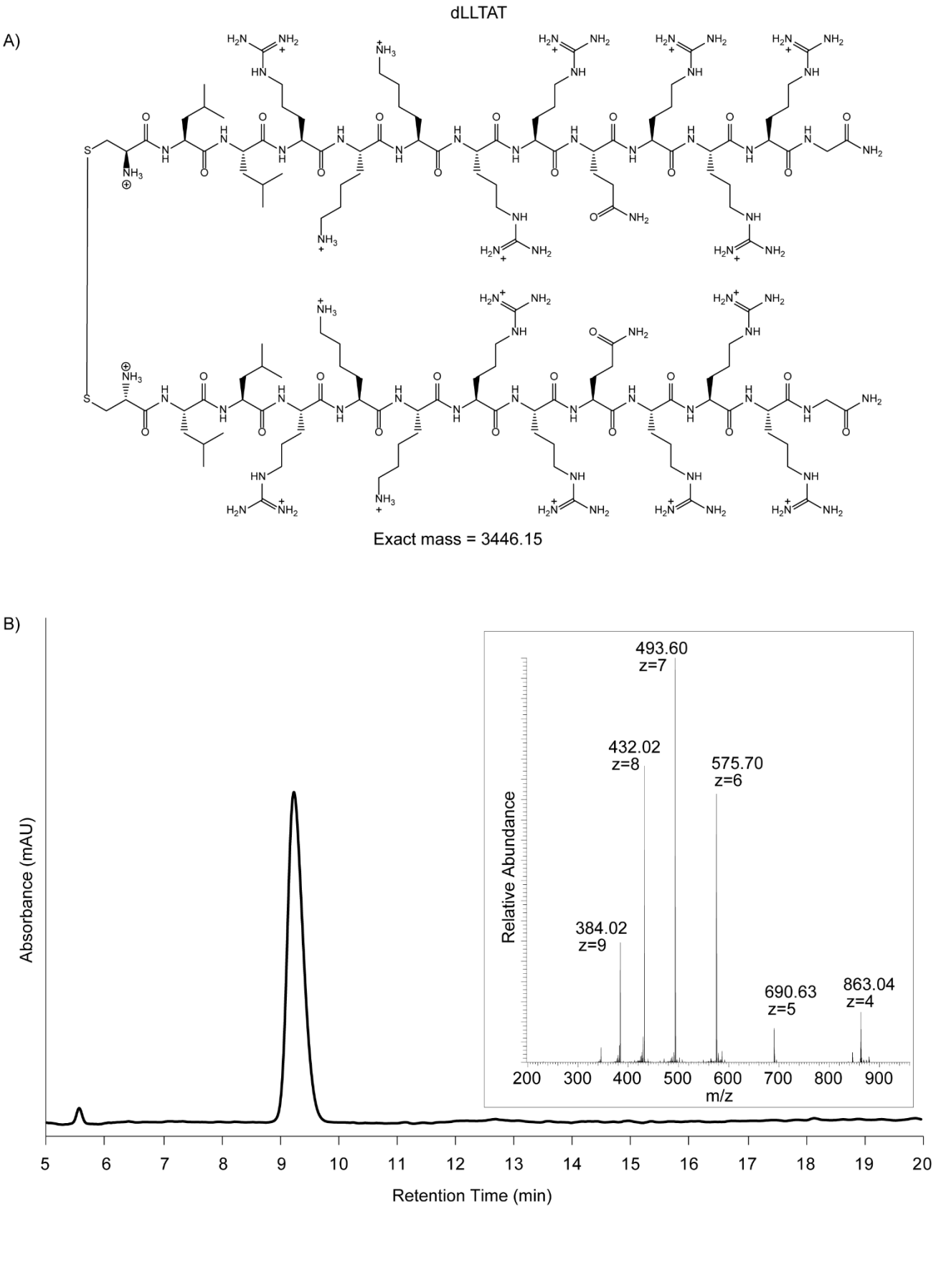
A)
dLLTAT
Exact mass = 3446.15
B)
Absorbance (mAU)
Retention Time (min)
Relative Abundance
m/z
493.60
z=7
432.02
z=8
575.70
z=6
384.02
z=9
690.63
z=5
863.04
z=4

Figure S30

d(HPV)TAT

A)

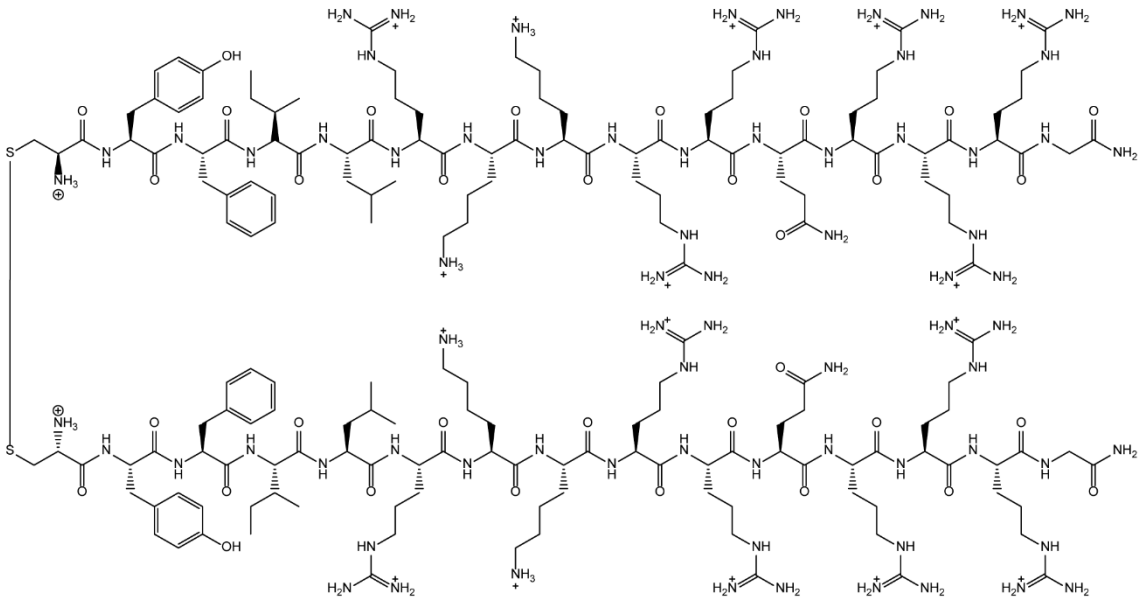

Exact mass = 4068.4

B)

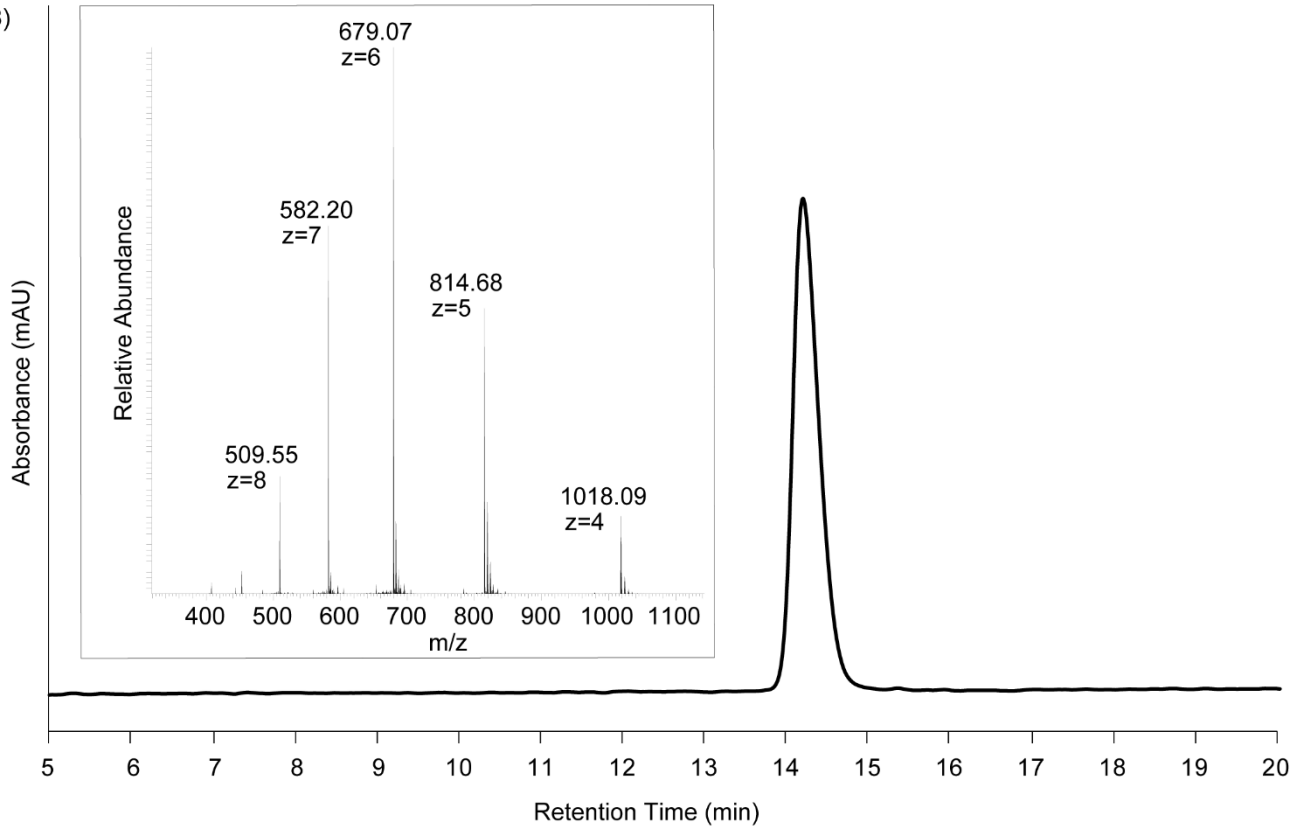

Figure S31

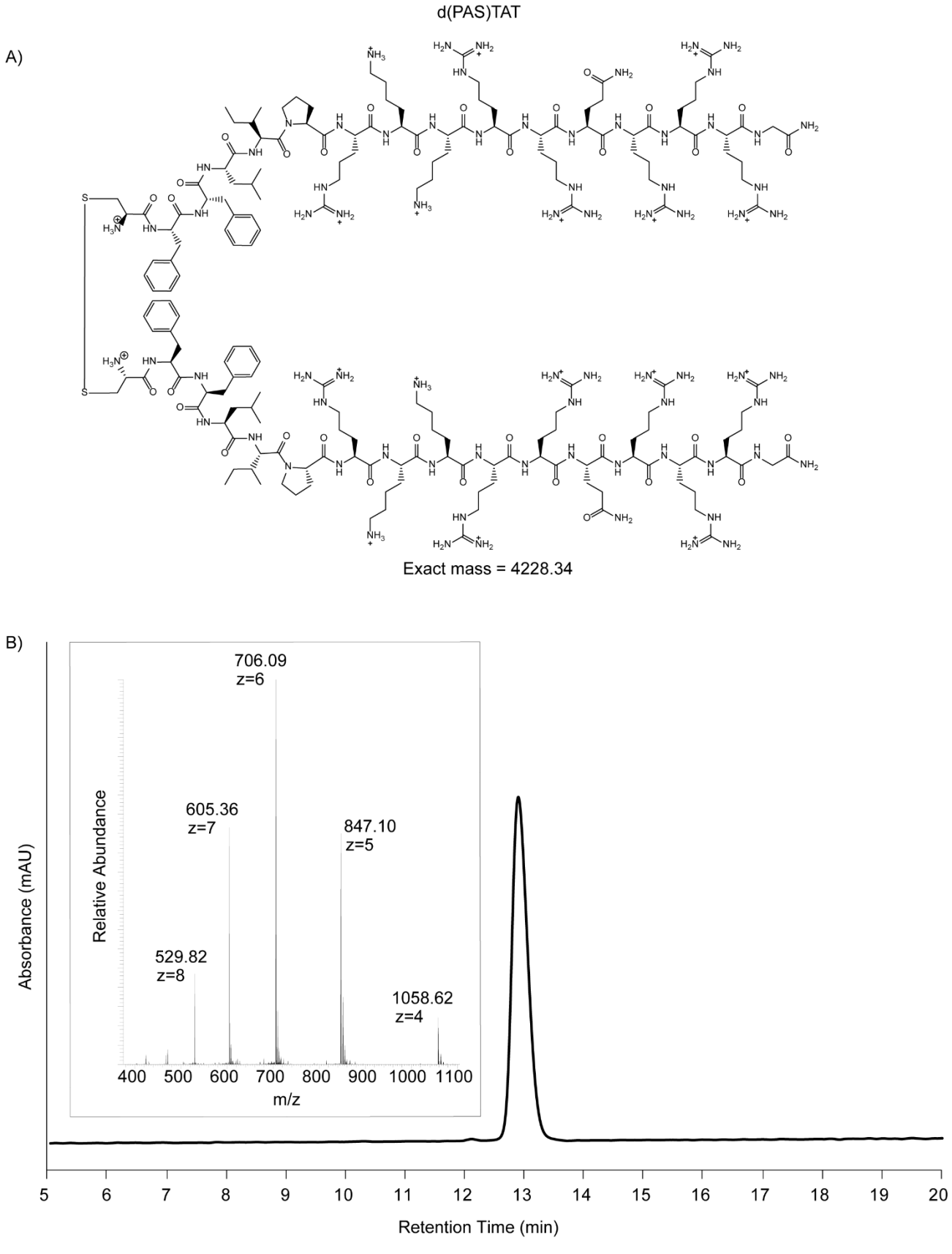
A)
d(PAS)TAT
Exact mass = 4228.34
B)
706.09
z=6
605.36
z=7
847.10
z=5
529.82
z=8
1058.62
z=4
Relative Abundance
m/z
Absorbance (mAU)
Retention Time (min)

Figure S23-S31. Peptide structures, purities, and mass. A) Structures, names and exact mass of all peptides used in this study. B) Peptide purity as analyzed by 214 nm absorbance via HPLC. Peptide masses were confirmed using electrospray ionization mass spectrometry.

Interpretation of nuclear extraction and quantification of delivered protein (Figures S10-S12, S17)

Figure 2 indicates that AF488-H1 and TAT-Cre reach the nuclei of cells when incubated with d(X)TAT peptides. In order to corroborate these results, we aimed to answer two questions: are the proteins that reach the nucleus intact, and how much intact protein is delivered by d(X)TAT? To answer these questions, nuclear extraction protocols were developed (Figures S10-S12). This protocol involves the permeabilization of the plasma membrane of cells with a mild detergent while cells adhere to plates, followed by washing of cytoplasmic components. The extracted nuclei were purified by sorting on a cell sorter, and their content was analyzed by either SDS-PAGE (with fluorescence detection for AF488-H1) or by western blotting (using anti-Cre monoclonal antibody). We detect that both AF488-H1 and TAT-Cre are present inside cells in the absence of d(WW)TAT (likely following endocytic uptake). Yet only the nuclei of cells incubated with d(WW)TAT contain detectable levels of protein payloads in their nuclei. The proteins are intact based on their molecular weight. We also estimate the nuclear protein concentration to be in the range of 1-10 μM. These estimates are based on SDS-PAGE/Western blot calibration curves established with known concentrations of proteins and by comparison of band intensities by densitometry analysis (the number of nuclei analyzed is also counted). In Figure S12, we provide a microscopy calibration experiment that corroborate these results with the fluorescence intensity of live cell nuclei stained by AF488-H1 being calibrated in the microscope independently of nuclear extraction protocols. Overall, these different approaches are in good agreement and demonstrated that d(X)TAT reagents deliver relatively high levels of intact proteins into the nuclei of live cells. Interestingly, these results also indicate that d(X)TAT does not change the total amount of material present in cells (this is consistent with both AF488-H1 and TAT-Cre being internalized by endocytosis, independently of d(X)TAT). Instead, d(X)TAT changes the localization of the protein payloads (from endosomes to nuclei).

These experiments involve multiple controls that address several questions: **1) are the nuclei pure and devoid of contaminants, 2) is the protein signal affected by the nuclear extraction process?**

Are the nuclei pure and devoid of contaminants? We first used AF488-H1 as a model as the fluorescence of the protein could be exploited to monitor every step of the nuclear extraction process. In Figure S11 we demonstrate by western blot that the nuclear extracts contain low levels of cytoplasmic contaminants using tubulin as a marker. Importantly, endolysosomes, which also contain AF488-H1 based on microscopy analysis, were removed by the nuclear extraction protocol as indicated by the absence of the endolysosome marker Lamp1. This was confirmed in Figure S10 where fluorescence microscopy shows that AF488-H1 puncta is removed from cells after extraction.

To remove extracellular AF488-H1 potentially sticking to the dish or to cells, cells were trypsinized and replated (as shown in Figure S11, trypsin degrades AF488-H1 within 1 min *in vitro*; trypsinized cells are exposed to trypsin for 5 min). The replating process also removed the majority of dead cells that may be stained with AF488-H1 after incubation with cells (Figure S13). Notably, this step required a delay in analysis as an additional 6 h were needed for live cells to adhere to new dishes. It is interesting to note that, during this waiting period, AF488-H1 is degraded in cells incubated with AF488-H1 alone, and to a lesser extent in cells incubated with d(WW)TAT. It is likely because AF488-H1 is subjected to rapid degradation by endosomal proteases while trapped inside endosomes/lysosomes (AF488-H1 alone condition). In contrast, upon escaping endosomes and reaching nuclei, AF488-H1 avoids rapid degradation (Figure S13 shows that the nuclear fluorescence of AF488-H1 persist in cells for at least 24 h).

To further purify the nuclear extracts, nuclei were sorted on a cell sorter. This was done to remove the few cells that may not have undergone permeabilization (<5% based on flow cytometry).

Is the protein signal affected by the nuclear extraction process? We first determined whether the membrane permeabilization process used to extract nuclei would alter the AF488-H1 signal detected in nuclei. In particular, we were concerned by two possibilities: the endosomal AF488-H1 may leak into nuclei during the extraction process, and, conversely, nuclear AF488-H1 may leak out of

nuclei. Both microscopy analysis (Figure S10) and flow cytometry (Figure S11) indicate that the signal of AF488-positive nuclei obtained after d(WW)TAT delivery is not substantially decreased by the extraction process. Likewise, cells incubated with AF488-H1 alone (showing only AF488-H1 puncta), do not display a nuclear signal before or after permeabilization. This is established in Figure S11, where the nuclei of cell incubated with AF488-H1 alone show no AF488-H1 signal by SDS-PAGE analysis. This absence of nuclear signal after cell permeabilization for this control was further confirmed by fluorescence microscopy in Figure S10. Based on these results, we conclude that the cell permeabilization protocol used to obtain nuclei does not contribute to apparent changes in the nuclear AF488-H1 signal.

Interpretation of d(X)TAT binding and diffusion (Figures S16 and S22)

The simple model provided in Figure S20A highlights that the injections performed *in vivo* could provide enough d(X)TAT reagent to achieve successful delivery in an area potentially as large as 3-4 mm in diameter. This is 4 times larger than the area of positive tdTom fluorescence observed in Figure 3. This analysis therefore highlights that d(X)TAT-mediated delivery remains relatively localized (albeit similar to AAV2). Please note that this simple analysis suffers from several limitations: 1) the volume injected is small and stereotactic injections can be imprecise in the volume delivered, 2) the concentration of d(X)TAT required for successful delivery (2.5 μM) is assumed based on the results of Figure 1, which requires 1h exposure to cells; however, the residence time of the peptide *in vivo* is currently unknown and could be much shorter. Nonetheless, we can speculate the diffusion of the peptide (and likewise TAT-Cre) is likely hindered *in vivo*. Likewise, several factors could lead to loss of activity (i.e. degradation). In Figure S16, we highlight how electrostatic interactions can both promote and inhibit delivery.

While the d(X)TAT reagents described in Figure 1 differ in position X, they share an arginine and lysine-rich peptide scaffold, with a total of 18 positive charges (12 R, 4 K, and 2 N-termini). The positive charges present in CPPs like TAT have been reported to play an important role in the binding to cell-surface heparan sulfate proteoglycans (HSPG) (*Biochemistry* **46**, 492-501). We have also reported on a cell penetration model where the polycationic dfTAT leaks out of late endosomes via interactions with the negatively charged lipid BMP (*Cell Chem Biol* **23**, 598-607; *Cell Chem Biol* **27**, 1296-1307 e1295). Overall, this suggests that electrostatic interactions with several anionic cellular partners (HSPG or BP) are important for the delivery activity of the peptide. In contrast, Figure S16 highlights how extracellular negatively charged species may inhibit delivery. These species may include soluble anionic glycosaminoglycans (as exemplified with heparin) or anionic proteins (as exemplified with albumin, pI of 4.5). The impact of albumin on dfTAT-mediated delivery has already been reported (*ACS Chem Biol* **14**, 2641-2651). Herein, we report the inhibitory effect of heparin. In this context, it is important to note that the payload used in this report, TMR-k5, AF488-H1, and TAT-Cre are polycationic. In particular, the isoelectric point of H1 is approximately 10.8, while that of Cre is 9.6 (based on the protein sequence and using the expasy pI computing tool found at https://web.expasy.org/cgi-bin/compute_pi/pi_tool).

Overall, the physical properties of d(X)TAT and its payload remain to be established *in vivo*. Based on our *in vitro* results, we can infer that d(X)TAT and payloads are not interacting to a significant extent during delivery. This is supported by the fact that no binding is detected in Figure S16 and, more importantly, by the fact that d(X)TAT delivers both TAT-Cre and H1 in the post-incubation format presented in Figure 2. Instead, it is likely that d(X)TAT binding to anionic extracellular components prevents the peptide from interacting with the cellular components important for delivery (e.g. HSPG and BMP), reduces the concentration of free peptide, and limits the amount of peptide that can mediate endosomal escape.

Methods:

Fluorescence Anisotropy. Fluorescence anisotropy was determined using a SLM-8000C fluorometer (SLM Instruments, Bath, UK) upgraded with the Phoenix package (ISS, Champaign, IL) and Vinci v.1.6 PC software (ISS). The contributions of light scattering and inner filter effect were minimized by filtering out the excitation wavelength from the emission beam and by using a low concentration of dfTAT (0.2 to 2 μM). Acquisition of fluorescence anisotropy was performed in 3 mm optical path micro-cuvettes over a ten second interval. Fluorescence anisotropy (*r)* was calculated automatically by Vinci v.1.6 PC software from four intensities of fluorescence measured under different positions of excitation and emission polarizers according to reported protocols (Ingersoll, C. M.; Strollo, C. M. *Journal of Chemical Education* 2007, *84*, 1313).

Titrations were repeated at least three times and average r values were determined for each data point. Fraction bound f_B was recalculated from anisotropy-concentration dependencies using the following equation:

$$f_B = \frac{r - r_F}{(r - r_F) + R \cdot (r_B - r)}$$

where r, rF and rB – respectively values of fluorescence anisotropy at a given titration condition, and for fully free or fully bound fluorophore (on start and saturation of titration). R is ratio of intensities of fluorescence of fully bound and fully free fluorophore forms, evaluated after correcting for dilution measured total fluorescence intensity values (determined by Vinci software in process of anisotropy calculation; derived from emission intensities for parallel and perpendicular polarizers orientations IVV and IVH as IVV +2·G·IVH, where G is the device-specific parameter)(Lakovicz, J. R. Principles of Fluorescence Spectroscopy; 3 ed.; Springer: Baltimore MD, 2006).

Peptide degradation assay. For degradation analysis in cells, either neuro2a or HeLa were washed three times with Leibovitz's nrL15 media (Fisher). Each well was simultaneously incubated with 5 μM of either L-amino acid or D-amino acid dfTAT. At various incubation time points, cells were washed two times with nrL15 supplemented with heparin (Sigma) (1 mg/mL) and one time with nrL15. For HPLC analysis, HeLa cells were extracted using 100 μL of a solution composing 75% acetonitrile, 23.5% water, and 1.5% TFA. The resulting extract was centrifuged at 21,000 x g for 10 min to remove insoluble debris prior to HPLC injection. For *in vitro* degradation analysis dfTAT and d(WW)TAT were incubated at 4 μM with ~1.5 units of Cathepsin B (Sigma C8571). Peptides were incubated with Cathepsin B at 37 ˚C for 24 hours at pH 5.5 in phosphate buffer. HPLC analysis was carried out on an Agilent HP 1200 series fitted with a Waters Acquity Protein BEH C4 column (2.1 mm x 100 mm) at 0.25 mL/min. For in-gel fluorescence analysis following incubation with peptides, Neuro2a cells were detached from the dish with a cell scraper and the cell suspension was lysed in 75 μL of lysis buffer (50 mM Tris-HCl, pH 7.5, 2 mM EDTA, 2 mM DTT, 0.1% Triton X-100, and HALT protease inhibitor). Lysates were freeze-thawed and treated with 1 μL DNase (Genesee) for 15 min on ice. Loading dye was added and lysates were boiled for 10 min at 100 °C. Finally, samples were run on a 16.5% Tris-Tricine gel (Bio-Rad cat# 3450063) using a running buffer composed of 100 mM Tris, 100 mM Tricine, and 0.1% SDS at pH 8.3 at 120 volts. Finally, gels were imaged for in-gel fluorescence and degradation was calculated by taking the ratio of low molecular weight bands containing a TMR fluorescent signal to the band intensity of reduced dfTAT, as analyzed by densitometry in ImageJ. Separate wells were also washed and imaged at 100X magnification to determine the localization of the TMR signal in cells overtime.

Quantification of TAT-Cre and AF488-H1 delivery into the nucleus of live cells. Following delivery of TAT-Cre or AF488-H1, cells were trypsinized and replated into fresh wells to remove any additional undelivered payload from the extracellular environment. Cells were then allowed to adhere once more to the plate prior to downstream processing. Once cells were adhered (apx. 6h), nuclei were extracted as described below. Following extraction, the nuclei were lysed in the well using lysis buffer (50 mM Tris-HCl, pH 7.5, 2 mM EDTA, 2 mM DTT, 0.1% Triton X-100, and HALT protease inhibitor). Whole-cell samples were treated identically with the omission of the nuclear extraction step. For TAT-

Cre, isolated nuclei from cells treated with either TAT-Cre alone or in the presence of peptide were run on SDS-PAGE and quantification was carried out by western blotting for Cre recombinase as described below. For quantitative determination of intact AF488-H1 inside the nucleus, isolated nuclei from cells treated with either AF488-H1 alone or in the presence of peptide were run using SDS-PAGE and analyzed for in-gel fluorescence (Typhoon FLA 9500).

Nuclear Extraction. Nuclear extraction was performed while cells were still adhered inside the well by replacing nrL15 with 100 µL of pre-extraction buffer (Abcam ab113474). After 8 minutes with frequent gentle swirling, the extraction solution was very gently removed from the cells and nuclei were imaged and subsequently lysed in-well for downstream analysis.

Interactions between peptide and protein. Peptides and protein were mixed into phosphate buffered saline (PBS) at 5 µM and 4 µM respectively. Samples were incubated at 37 ˚C for 1 hour, then mixed with SDS-PAGE loading dye in the absence of reducing agent and left unboiled. Samples were run using SDS-PAGE and imaged for in-gel fluorescence and Coomassie staining (Typhoon FLA 9500). For the penetration of dfTAT in the presence of heparin, HeLa cells were incubated with 5 µM dfTAT at various concentrations of heparin. After a 1 h incubation cells were washed and imaged at 100x and 20x for quantification of peptide penetration.

SDS-PAGE and western blotting. Samples were run on 4-20% tris-glycine gels (Invitrogen) at 130 V. For western blotting, proteins were transferred to a PVDF membrane (Amersham Hybond) at room temperature for 2 hours at 75 V. Membrane was blocked for 1 hour in 5% BSA in TBST (50 mM Tris-HCl, 150 mM NaCl, 0.1% Tween-20 at pH 7.4). Anti-lamin B1 (A-11) (Santa Cruz Biotechnology), anti-alpha tubulin (DM1A) (Abcam), anti-Lamp1 (D2D11) (Cell Signaling Technology) and/or horse radish peroxidase-conjugated anti-Cre Recombinase (D7L7L) (Cell Signaling Technology) were incubated at a 1:1000 dilution in 1% BSA in TBST overnight at 4 °C. The following day membranes were washed with TBST and those requiring secondary antibodies for detection were subsequently incubated with a horseradish peroxidase-conjugated secondary antibody (BD Biosciences #554002 / #554021) at room temperature for 1 hour. Membranes were washed with TBST once more followed by water. Finally, membranes were incubated with SuperSignal West Pico PLUS Chemiluminescent Substrate (Thermo) for 5 min before imaging on an Amersham 600 imager set to auto exposure on the chemiluminescence setting.